Dissertation

submitted to the

Combined Faculty of Natural Sciences and Mathematics

of the Ruperto Carola University Heidelberg, Germany

for the degree of

Doctor of Natural Sciences

Presented by

M.Sc. Shehabeldin Elzoheiry

born in: Kuwait

Oral examination: 28th of October 2019

Mild metabolic stress is sufficient to disturb the formation of pyramidal cell ensembles during gamma oscillations

Referees: Prof. Dr. Hilmar Bading

Prof. Dr. med. Andreas Draguhn

Abstract

Gamma oscillations are associated with several higher cognitive functions; selective attention, memory formation, and sensory perception. Gamma oscillations represent a balanced fast interplay between excitation and inhibition. Inhibition provides temporal windows for excitatory cells to fire in synchrony. Whether excitation or inhibition requires more energy is still unknown. Disturbances of gamma oscillations occur rapidly during metabolic stress. However, the underlying mechanisms are not fully understood. In this study, we performed calcium imaging (CamKII.GCaMP6f) to explore the presence of pyramidal cell ensembles in rat hippocampus and challenge them metabolically. Using a low concentration of rotenone we achieved a mild metabolic stress condition. The stress level results in suppressing gamma oscillations without being terminated. We found that (1) synchronized activity is significantly reduced before observing a reduction in the overall activity of pyramidal cells. (2) Pyramidal cells recruited in ensembles formation tend to be more active upon mild stress. We performed spike sorting and found that (3) slow-spiking units are more active upon mild metabolic stress. Furthermore, (4) power of gamma oscillations was reduced without changes in the firing of fast-spiking units. These findings suggest that ensemble formation is highly vulnerable to metabolic stress, and disturbances occur likely because of functional alterations in the presynaptic compartment of fast-spiking units. This reveals a plausible mechanism for altered cognitive functions during mild metabolic stress conditions.

Zusammenfassung

Gamma-Oszillationen werden bei verschiedenen höheren kognitiven Leistungen beobachtet: selektive Aufmerksamkeit, Gedächtnisbildung und sensorische Wahrnehmung. Gamma-Oszillationen hängen von einem ausgewogenen Zusammenspiel von erregenden und hemmenden Einflüssen ab. Die Hemmung bietet zeitliche Fenster, in denen exzitatorische (Pyramiden)zellen synchron feuern können. Es ist noch nicht bekannt, ob die erregenden oder hemmenden Zellen mehr Energie benötigen. Störungen von Gamma-Oszillationen treten schnell bei metabolischer Belastung auf. Die zugrunde liegenden Mechanismen sind jedoch nicht vollständig verstanden. In dieser Studie haben wir Calcium-Imaging (CamKII.GCaMP6f) durchgeführt, um im Hippocampus der Ratte die Existenz von Ensembles aus Pyramidenzellen nachzuweisen und die Auswirkungen von metabolischer Belastung zu untersuchen. Dazu haben wir eine niedrige Konzentration von Rotenon verwendet, die die Intensität der Gamma-Ozillationen schwächt ohne sie ganz zu unterdrücken. Wir fanden heraus, dass (1) die synchronisierte Aktivität von Pyramidenzellen signifikant reduziert ist, ohne dass sich deren Gesamtaktivität verändert. (2) Pyramidenzellen, die bei der Bildung von Ensembles rekrutiert wurden, werden bei leichtem Stress aktiver. Die nähere Analyse des Spikeverhaltens (Generation von Aktionspotentialen) der beteiligten Zellen ergab, dass (3) langsam spikende Zellen bei metabolischem Stress aktiver sind. Darüber hinaus wurde (4) die Intensität der Gamma-Oszillationen vermindert, ohne dass sich die Aktivität schnell spikender Zellen verändert. Diese Ergebnisse deuten darauf hin, dass die Ensemblebildung sehr anfällig für metabolischen Stress ist und Störungen wahrscheinlich durch funktionelle Veränderungen im präsynaptischen Bereich von schnell spikenden Zellen auftreten. Die Daten können die Veränderung kognitiver Fähigkeiten bei (leichten) metabolischen Stressbedingungen erklären.

Declaration

I, Shehabeldin Elzoheiry, hereby declare that the work in this thesis represents my original research results. The thesis has been written by myself using the references and resources indicated. Any work of others has been appropriately marked. The work has been conducted under the joint supervision of Prof. Dr. Hilmar Bading and Prof. Dr. med. Andreas Draguhn. This thesis is being submitted for the degree of Doctor of Natural Sciences at Heidelberg University, Germany, and has not been presented to any other university as part of an examination or degree.

_____   _____

Place & Date   Shehabeldin Elzoheiry

Parts of this work that were done by others:

*Organotypic hippocampal slice cultures were prepared by Andrea Lewen.

*Calculations of cerebral metabolic rates were performed by Dr. Nikolaus Berndt.

Parts of this work were presented in the following conferences:

      -IZN retreat 2019 (Poster).

      -NWG 2019 - 13th Göttingen Meeting of the German Neuroscience Society (Poster).

      -IZN retreat 2018 (Poster).

      -IZN retreat 2017 (Poster).

      -NWG 2017 - 12th Göttingen Meeting of the German Neuroscience Society (Poster).

      -IZN retreat 2016 (Poster).

List of abbreviations

AAV5	Adeno-associated virus serotype 5
ACSF	Artificial cerebrospinal fluid
AD	Alzheimer's disease
AMPA	α-amino-3-hydroxy-5-methyl-4-isoxazolepropionic acid
AP	Action potential
ATP	Adenosine triphosphate
AuC	Area under the curve
CA	Cornu ammonis
CaMKII	Ca^{2+}/calmodulin-dependent protein kinase II
CCH	Carbachol
$CMRO_2$	Cerebral metabolic rate of oxygen
DG	Dentate gyrus
DIV	Days *in vitro*
DL-AP5	DL-2-Amino-5-phosphonopentanoic acid
DNQX	6,7-Dinitroquinoxaline-2,3-dione
f	Frequency
FFT	Fast Fourier transform
FWHM	Full width at half-maximum
GABA	Gamma-Aminobutyric acid
GAD	Glutamic acid decarboxylase
GAT	Gamma-Aminobutyric acid transporters
GECI	Genetically encoded calcium indicator
ISI	Inter-spike interval
LFP	Local field potential
OHSC	Organotypic hippocampal slice culture
PC	Principal component
PCA	Principal component analysis
PSD	Power spectral density
PV	Parvalbumin
Pyr	Pyramidale
Rad	Radiatum
ROI	Region of interest
Rot	Rotenone
SEM	Standard error of the mean
SV40	Simian vacuolating virus 40
TTX	Tetrodotoxin
WPRE	Woodchuck Hepatitis Virus Posttranscriptional Regulatory Element

Table of contents

1 Introduction

1.1 Neuronal Ensembles

The Human brain is composed of around 100 billion neurons, which are the most complex mammalian cells. Each cell is involved in at least 1000 innervations with other neurons, resulting in 100 trillion connection points, synapses (Herculano-Houzel, 2009; Kandel et al., 2012; Williams and Herrup, 1988). These synapses are plastic, endowing the brain with an unlimited number of paths for transferring information. The unlimited paths for information transfer highlight one prominent feature of the nervous system, which is its connectivity (Cajal, 1899).

The nervous system is capable of exhibiting reproducible adaptive behaviors (Ardiel and Rankin, 2010; Whishaw and Kolb, 2004). The explanation for how reproducible behavior can emerge from such a system is the presence of specific cells (spatial pattern) firing within a certain time frame (temporal pattern; Figure 1). This sheds light on the presence of reproducible patterns of neuronal activity underlying behavior. These patterns result from co-active neurons, which define the term 'ensembles'. Other terms exist in the literature, such as neuronal avalanches and attractor states (Durstewitz et al., 2010; Grillner and Wallen, 1985; Ikegaya et al., 2004; Lin et al., 2006; Plenz and Thiagarajan, 2007). However, the ensemble is the umbrella term for a transiently stable group of neurons that are repetitively active. It is believed that ensembles are bridging between single-cell activity and emerging higher cognitive functions such as memory, attention, and perception (Buzsáki, 2010).

Combinatorial explosion is an important output of the ensemble concept. With the recruitment of groups of co-active neurons, the computational representation of information expands enormously, a necessary feature for the functioning of a complex organ like the brain (Ainsworth et al., 2012; Ohiorhenuan et al., 2010; Olshausen and Field, 2004).

Structural and functional properties of neuronal networks are highly heterogeneous, however, common principles exist. Principles include homeostasis (Kann et al., 2016; Zenke et al., 2013), sparsity, local connectivity, and temporal organization. Homeostasis indicates the preservation of excitation-inhibition balance thus avoiding pathological activity (Ingram et al., 2014; Nanou et al., 2018; Rubin et al., 2017). Sparsity refers to the low percentage of cells being active at a time point, which is an energy-efficient model for information transfer (Ainsworth et al., 2012; Buzsáki and Draguhn, 2004; Ohiorhenuan et al., 2010).
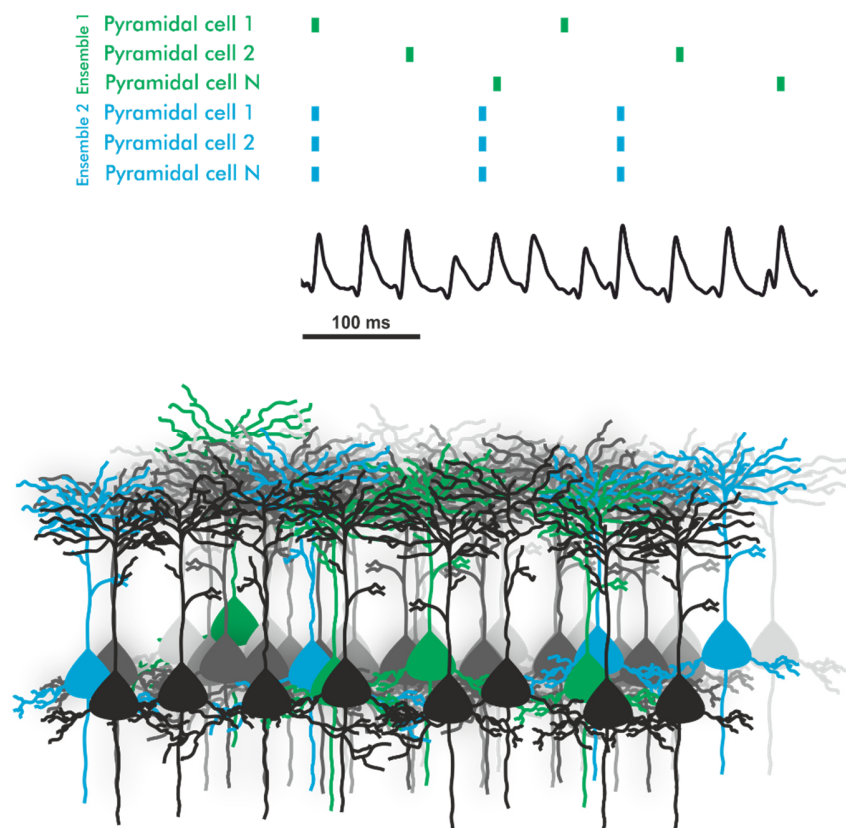
Figure 1. Schematic drawing of ensembles during network activity. Blue and green ensembles represent two different possibilities for temporal matrices. Neurons recruited in an ensemble can have sequential firing pattern (green) or simultaneous (blue) or a mixture of both. Black trace represents a gamma oscillation epoch of the network, a state where it is believed that neurons fire in a synchronized pattern.

1.1.1 Basic features of neuronal ensembles

1) **Selective coupling**, implying that neurons recruited in an ensemble have privileged connections. This is crucial for having temporal matrices were individual neurons know when to fire action potentials in synchrony with other members of the same ensemble (Hoshiba et al., 2017).

2) **State-dependent activity**. A neuronal ensemble can be activated in different network states, thereby executing different functions depending on the context. For instance, during theta-gamma activity, an ensemble may contribute to the formation of a new memory (Backus et al., 2016; Nyhus and Curran, 2009). The same ensemble can be involved in memory consolidation during sharp-wave ripples (Joo and Frank, 2018; Olafsdottir et al., 2018).

3) **Region-specific activity**. Properties of ensembles may be different between local networks. Ensembles identified in the dentate gyrus are composed of neurons that fire sparsely, which is fundamental for a major function in the dentate gyrus, pattern separation (Berron et al., 2016; Faghihi and Moustafa, 2017; Leutgeb et al., 2007; Leutgeb and Leutgeb, 2007). On the contrary, ensembles detected in the CA3 region are composed of neurons that are not sparsely firing, which are involved in pattern completion (Guzman et al., 2016; Leutgeb and Leutgeb, 2007; Leutgeb et al., 2006; Rolls, 2013).

4) **Network plasticity**. An ensemble of neurons can be assembled rapidly during the exploration of a new environment encoding spatial information. For this to be accomplished, networks should be adaptable and plastic for the unlimited number of new environments that can be explored (Hoshiba et al., 2017; Neves et al., 2008; Zarnadze et al., 2016).

5) **Background suppression**. During activation of a certain ensemble, other non-recruited neurons should be silenced. The suppression ensures that the output has a sufficient signal-to-noise ratio. This feature sheds light on the important role of inhibitory interneurons during the formation of neuronal ensembles (Bartos et al., 2007; Kann et al., 2014).

1.1.2 Neuroenergetics and ensembles formation

Recruitment of neurons into ensembles require selective activation, which involves informing neurons when they are supposed to fire action potentials and when to be silenced. From neuroenergetics perspective, it is believed that suppression of background during synchronized network activity costs much energy (Kann et al., 2014). These costs may set boundaries for eliciting structured activity patterns (Sengupta et al., 2013). Studying the neuroenergetics underlying formation of neuronal ensembles favors understanding bigger concepts and questions regarding the interpretation of functional neuroimaging (Attwell and Iadecola, 2002).

1.2 Neuroenergetics of Neuronal Ensembles

The mammalian brain is a highly active organ. In adult humans, 20% of the utilized oxygen is consumed by the brain, although contributing only 2% to the total body mass (Erecińska and Silver, 2001; Rolfe and Brown, 1997). Indicating that information processing requires high energy budget. This explains the vulnerability of higher brain functions to metabolic stress (Hansen, 1985; Kann, 2012; Shulman et al., 2001; Verweij et al., 2007). The energy budget includes costs of resting membrane potential, action potentials, postsynaptic potentials and neurotransmitter metabolism (Harris et al., 2012; Kann, 2012).

Studies on brain energy metabolism have focused mainly on broad aspects. This includes the energy budget of excitatory neuronal signaling (Attwell and Laughlin, 2001; Lutas and Yellen, 2013; Martinez-Francois et al., 2018), the favorable energy substrate for neurons (Chih et al., 2001; Díaz-García et al., 2017; Diaz-Garcia and Yellen, 2019; Erecińska and Silver, 2001), and the contributions of glycolysis and oxidative phosphorylation to ATP generation (Yellen, 2018). Important aspects of brain energy metabolism, that are still largely unknown, is the vulnerability of inhibitory and excitatory neurons to metabolic stress. This question is made challenging due to the difficulty of dissecting the network into excitatory and inhibitory cells and determining afterwards the energy budget for individual populations.

1.2.1 Interneuron energy hypothesis

Inhibitory cells play a fundamental role in synchronizing activity patterns of principal cells. Among several types of interneurons, fast-spiking basket cells appear to be an interesting candidate for neuroenergetics studies (Gulyás et al., 2010; Kann, 2016). Previous studies have shown that fast-spiking interneurons are equipped with a large number of mitochondria. Furthermore, mitochondria were found to be enriched with cytochrome C and cytochrome C oxidase, also known as complex IV (Gulyás et al., 2006; Kageyama and Wong-Riley, 1982). This indicates that fast-spiking interneurons consume much energy, which implies that they might be sensitive to mild metabolic insults. Energy is consumed in several processes (Kann, 2016), such as the following:

1.2.1.1 Fast-spiking behavior

The high firing rate is enabled by several properties of the interneurons. Their resting membrane is ~10-15 mV closer to firing threshold in comparison to principal cells (Hu et al., 2014; Hu and Jonas, 2014). Additionally, they show resonance at beta-gamma frequencies (Pike et al., 2000).

1.2.1.2 Presynaptic GABA release

At the presynapse, GABA is required to be recycled at a very high rate to cope with fast signal transmission required for the arriving action potentials. Recycling includes the fast and efficient release of the transmitter, reuptake, and vesicles filling (Roth and Draguhn, 2012).

Endowed by the tight coupling of release sensors and calcium channel composition, GABA release is characterized by high release probability and large quantal size (Bucurenciu et al., 2008; Kraushaar and Jonas, 2000). Re-uptake of GABA includes the activity of GABA-transporter-1 (GAT-1) in presynaptic terminal and GAT-3 in astrocytes enwrapping synaptic clefts. The vesicular filling includes the activity of one of the two glutamic acid decarboxylase (GAD) isoforms, which is GAD-65. Additionally, it includes the activity of vesicular H^+-ATPase which provides the driving force required by the vesicular GABA transporter (Bak et al., 2006; Roth and Draguhn, 2012; Waagepetersen et al., 2001; Walls et al., 2011).

These are secondary-active processes, which depend on gradients produced by Na^+/K^+-ATPase pump and other transporters. All processes depend on ATP whether directly or indirectly (Attwell and Laughlin, 2001; Rangaraju et al., 2014).

1.2.1.3 Postsynaptic effect

Inhibitory conductance involves chloride influx in large postsynaptic population innervated by the highly branched axon. Fast-spiking interneurons that are involved in fast-brain oscillations, target the perisomatic region (Hájos and Paulsen, 2009). Restoration of ion gradients across postsynaptic membrane involves activity of several transporters e.g. the secondary-active transporter, K^+/Cl^- cotransporter (Chamma et al., 2012; Kann, 2016).

1.2.2 Metabolic stress

Stressing the formation of neuronal ensembles mildly might reveal the most vulnerable population to energy restriction: inhibitory or excitatory neurons. Stress can be achieved by several means. This includes reduced oxygen supply or nutrients such as glucose or by application of toxins such as rotenone (Galow et al., 2014; Kann et al., 2011), which is a highly selective inhibitor of complex I of the mitochondrial respiratory chain (Sherer et al., 2003), thereby partially blocking the synthesis of ATP.

Homeostasis endows biological materials with versatility in facing disturbing environmental conditions (Kann et al., 2016; Vodovozov et al., 2018). Therefore to study break down of a function, the biological material has to be stressed severely. An alternative would be the induction of mild stress while setting the biological matter to function near its limits. Gamma oscillations represent a brain state associated with high energy consumption (Kann, 2012, 2016; Kann et al., 2011; Kann et al., 2014; Schneider et al., 2017). Therefore, modeling gamma oscillations can simulate thrusting the brain tissue to the limits, and further induction of mild metabolic stress can reveal mechanistically the collapse of the network, helping to understand the underlying physiology.

1.3 Gamma Oscillations

Different brain activities and rhythms are associated with a wide range of higher cognitive functions such as attention, memory formation, and consolidation, etc. (Buzsáki and Draguhn, 2004; Colgin, 2016; Paulsen and Moser, 1998; Uhlhaas and Singer, 2010). Here we focus on gamma oscillations, which represent the oscillatory activity in the frequency band of 30-100 Hz (Buzsáki and Wang, 2012).

Several regions of the brain are known for expressing gamma oscillations. These include striatum (Berke et al., 2004; Tort et al., 2008), amygdala (Halgren et al., 1977; Popescu et al., 2009), entorhinal cortex (Chrobak and Buzsáki, 1998), olfactory bulb (Adrian, 1942), hippocampus, neocortex (Buzsáki et al., 1983; Whittington et al., 1995), and thalamus (Pinault and Deschenes, 1992).

These oscillations are known to be associated with several complex brain functions, including selective attention and sensory perception (Bartos et al., 2007; Kann et al., 2014; van Vugt et al., 2010). Gamma oscillations provide the temporal matrix necessary for synchronizing the neuronal activity, which is required for these functions to arise (Haider and McCormick, 2009; Mainen and Sejnowski, 1995).

Synchronization of several neurons' output results in fluctuations of summed postsynaptic potentials. These subthreshold summed activities can be sensed in local field potentials using an extracellular electrode. The gamma oscillations waveform emerges from the fluctuation of synaptic potentials which results from the interplay between excitatory principal cells and inhibitory interneurons (Hájos and Paulsen, 2009). The fluctuations reflect time windows of increased and reduced excitability in the targeted population (Buzsáki et al., 1983; Soltesz and Deschenes, 1993). These time windows are necessary for recruiting targeted population into ensembles, which play an important role in information processing (Poschel et al., 2002).

There are two underlying models for the generation of gamma oscillations, inhibition-inhibition and excitation-inhibition models (Buzsáki and Wang, 2012).

1.3.1 Inhibition-inhibition model

The inhibition-inhibition model involves repetitive cycles of inhibition between mutually connected inhibitory interneurons. This results in cycles of inhibitory postsynaptic potentials, IPSPs, which underlie the gamma oscillation waveform. The frequency of the oscillations in this model is determined by the subunit composition of GABA receptors which govern the duration of IPSPs (Wang and Buzsáki, 1996; Whittington et al., 1995).

1.3.2 Excitation-inhibition model

The excitation-inhibition model includes the coordinated activity of pyramidal cells (excitatory) and interneurons (inhibitory). The frequency of the oscillations in this model is determined by the delay between pyramidal and interneuron spikes, caused by axonal conduction and synaptic delays (Borgers and Kopell, 2003; Brunel and Wang, 2003; Ermentrout and Kopell, 1998; Geisler et al., 2005; Leung, 1982; Wilson and Cowan, 1972).

1.3.3 Gamma oscillations in the hippocampus

In the hippocampus, principal cells reside in a special laminated architecture, contrary to other cortical regions. This architecture favors the summation of population activity. Therefore, gamma oscillations detected in the hippocampus show higher power compared to signals detected in other brain regions, where cells do not reside in similar spatial configuration (Forster et al., 2006).

Pyramidal cells in the hippocampus are the principal excitatory cells which are known to compute, store and retrieve information (Uhlhaas and Singer, 2010). These are fundamental tasks that underlie information processing and higher cognitive functions. During gamma oscillations, the excitatory output is synchronized and consequently, pyramidal cells are recruited into ensembles. Therefore, gamma oscillations play an important role in cortical information processing (Engel et al., 2001).

The fact that gamma oscillations are detected in the hippocampus during specific behaviors rendered the hippocampus an interesting model to study the relation between neuronal network activity and behavior (Bragin et al., 1995). Additionally, since the hippocampus is involved in navigation and memory, the study of network activity will relate to coding, storage, and retrieval

of information (Lisman, 1999; O'Keefe and Recce, 1993; Skaggs et al., 1996). Combined together, these intrinsic properties of the hippocampus depicted it as an appealing model to study gamma oscillations.

1.3.4   *In situ* chemical models of gamma oscillations

Gamma oscillations can be induced *in situ* by different means, including electrical stimulation, application of chemical agonists or optogenetic stimulation. Chemical induction includes agonists of metabotropic glutamate receptors, muscarinic acetylcholine receptors, kainate receptors, and even potassium salt solutions. Nevertheless, the synaptic activity and balance of excitation and inhibition underlying gamma oscillations are different in each model (Fellous and Sejnowski, 2000; Fisahn et al., 2004; Fisahn et al., 1998; Hájos et al., 2000; LeBeau et al., 2002; Whittington et al., 1995).

1.3.5   Glutamatergic and cholinergic gamma oscillation models

Metabotropic glutamate receptors and kainate receptor-induced gamma oscillations (glutamatergic model) were found to be blocked by bicuculline ($GABA_A$ receptor blocker). However, AMPA receptor blockers did affect the oscillations (Fisahn et al., 2004).

Gamma oscillations induced by carbachol (cholinergic model) resemble the glutamatergic model of gamma oscillation in which the oscillations are abolished by $GABA_A$ receptor blockers. However, they are affected by AMPA receptor blocker. Cholinergic model is employed in many studies because it simulates inputs of the septum to the hippocampus when gamma oscillations are detected *in-vivo*.

Based on previous studies, it is believed that metabotropic glutamate receptors and kainate receptors activate interneurons and muscarinic acetylcholine receptors activate principal cells. Therefore, glutamatergic gamma oscillation model is not based on phasic excitation which is necessary for activating interneurons in the cholinergic model (Fisahn et al., 2004; Fisahn et al., 2002; McBain et al., 1994; van Hooft et al., 2000).

In conclusion, glutamatergic gamma oscillation model is dependent on inhibition but not excitation, while cholinergic models are based on both (Figure 2). As a result, the differences in
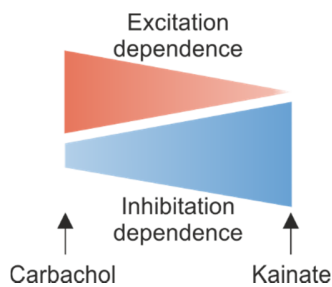
Figure 2. Schematic diagram for dependence of gamma oscillation models on excitation and inhibition. Cholinergic models are based on both excitation and inhibition while glutamatergic models are based on inhibition. Modified after Bartos et al. 2007

these models can be utilized to study the contribution of excitation and inhibition underlying activity of gamma oscillations (Bartos et al., 2007).

1.3.6 GABAergic interneurons

GABAergic interneurons constitute around 10 to 20% of neurons in cortical circuits. The rest are principal cells, which are usually glutamatergic (Aika et al., 1994; Freund and Buzsáki, 1996; Halasy and Somogyi, 1993). Interneurons are considered to be the 'brakes' that control principal cells activity in the brain. This maintains a physiological excitation-inhibition balance which protects from pathological activity such as seizures and loss of cognitive functions (Hermann and Seidenberg, 2007; Lenck-Santini and Scott, 2015).

In the hippocampus, more than twenty types of interneurons are identified. They are categorized based on different properties. 1- Morphological features and targeted compartments in innervated cells (dendritic, somatic, axonic). 2- Calcium-binding proteins (parvalbumin, calbindin, etc.) or neuropeptides (cholecystokinin, somatostatin, etc.) that are expressed. 3- Functional features such as firing rates and adaptation. However, classifications often result in the overlapping categorization of interneurons (DeFelipe et al., 2013; Somogyi and Klausberger, 2005).

Among these types, fast-spiking PV+ interneurons are particularly of main interest when studying gamma oscillations. These cells are believed to be essential for the generation of gamma oscillations. Fast-spiking interneurons fire action potentials that are highly coherent to the gamma

oscillation cycle. These spikes occur few milliseconds after the firing of neighboring pyramidal cells. In pyramidal cells, inhibitory postsynaptic potentials are phase-locked to gamma oscillation cycles. (Hasenstaub et al., 2005; Mann et al., 2005; Penttonen et al., 1998; Soltesz and Deschenes, 1993; Whittington et al., 1995). These subthreshold fluctuations shape the gamma oscillation waveform (Gloveli et al., 2005; Hasenstaub et al., 2005; Mann et al., 2005; Penttonen et al., 1998; Quilichini et al., 2010).

Further support for the role of fast-spiking interneurons in generating gamma oscillations is the induction of gamma oscillations by optogenetic stimulation of PV+ cells. The oscillations power were even reduced when PV+ cells were inhibited (Bartos et al., 2007; Cardin et al., 2009; Sohal et al., 2009). Additionally, fast-spiking interneurons show a resonant property in the range of gamma-band frequencies (Cardin et al., 2009).

The ability to maintain high firing rates during gamma oscillations, indicate that fast-spiking interneurons are endowed with special molecular and morphological features to perform such function.

1.3.6.1 Dendritic features

Fast-spiking interneurons sample inputs and integrate information from a large number of principal cells (16000 ~ 34000 synapses) along their long dendritic tree (Gulyas et al., 1999; Tukker et al., 2013). The dendrites are equipped with a low density of voltage-gated Na+ channels. On the contrary, they have a high density of voltage-gated K+ channels. Potassium channels are of the Kv3 type, which has a high activation threshold, fast activation and deactivation kinetics (Rudy and McBain, 2001). Thus the composition of ion channels enables fast decay of excitatory postsynaptic potentials, consequently, the time available for temporal summation is shortened. Therefore, these cells are able to generate action potentials with high temporal precision and at very high rates.

1.3.6.2 Axonal features

Axons form a highly branched arbor at the peri-somatic region, like baskets, hence the name basket cells. These cells show a unique distribution of Na+ channels along their axons. There is a

decremental increase in the channels density from soma towards distal axons reaching 'supercritical' densities (Hu and Jonas, 2014; Martina and Jonas, 1997). This ensures high reliability of propagation and firing rates. Additionally, it compensates for the small diameter of unmyelinated axons, and extensive arborization which acts against maintaining reliable action potential propagation (Parnas and Segev, 1979).

Furthermore, the axons contain Kv3 channels similar to the dendrites (Goldberg et al., 2005; Hu and Jonas, 2014). Therefore, they are able to maintain high firing rates with high temporal precision (Weiser et al., 1995).

1.3.6.3 Presynaptic terminal

Fast-spiking is retarded by synaptic delay, however, basket cells are equipped with proper machinery to minimize this delay.

The presynaptic terminal contains mainly P/Q-type Ca^{2+} channels (Bucurenciu et al., 2010; Hefft and Jonas, 2005; Rossignol et al., 2013; Zaitsev et al., 2007), which has the fastest gating in comparison to other Ca^{2+} channels (Li et al., 2007). Additionally, Ca^{2+} channels are tightly coupled to release sensors (in the range of 10-20 nm) at the presynaptic terminal (Bucurenciu et al., 2008; Eggermann et al., 2011). Furthermore, the number of channels per release site is low (2 ~ 3 channels), thus limiting any broadening of action potentials (Bucurenciu et al., 2010). Combined together, all these features result in fast signal transmission with high efficacy and temporal precision (Bucurenciu et al., 2008).

Fast-spiking cells are not only involved in simple control of principal cells' excitation but are rather involved in feedback and feedforward inhibition, which play an important role on the network level. For instance, feedforward inhibition enhances the temporal resolution for summation of postsynaptic potentials and initiation of action potentials, thereby broadening the dynamic range of neuronal ensembles (Pouille et al., 2009; Pouille and Scanziani, 2001).

1.4 Aims

Disturbances of cognitive functions occur rapidly during metabolic stress. However, the underlying mechanisms are not fully understood. Alterations of gamma oscillations have been studied so far at the network level (Huchzermeyer et al., 2008; Huchzermeyer et al., 2013; Kann et al., 2011; Schneider et al., 2017). Here, it was aimed to study the alterations at the level of neuronal ensembles, which can bridge between disturbances at the cellular level and altered cognitive functions.

In this study, it is hypothesized that:

- Pyramidal cell ensembles exist during induction of gamma oscillations.
- Formation of pyramidal cell ensembles is sensitive to metabolic stress.
- Inhibitory function during gamma oscillations is energetically more demanding than excitatory function.

To test these hypotheses, the following aims were addressed.

- Detection of pyramidal cell ensembles.
  - This was fulfilled by performing calcium imaging, which enabled monitoring activity of a large number of neurons simultaneously. Moreover, analytical methods for the detection of synchronized activity were employed to detect co-active neurons (ensembles) with repetitive patterns of activity.
- Determination of metabolic stress condition to challenge gamma oscillations.
  - The stress level should be mild in comparison to previous studies (Huchzermeyer et al., 2008; Huchzermeyer et al., 2013; Kann et al., 2011). Additionally, it should be sufficient to attenuate gamma oscillations without inducing pathological activity (spreading depolarization or epileptiform discharges).
- Determination of cerebral metabolic rates in different models of gamma oscillations.
  - This was achieved by performing oxygen depth profiles using Clark-type oxygen microsensors. The plan was to utilize the difference in the balance of dependence on inhibition and/or excitation of different models (cholinergic and glutamatergic).

13

This was planned to enable investigating whether inhibition or excitation costs more.

- Performing spike sorting on units detected during gamma oscillations.
  - This was applied to provide insight about changes in firing behavior upon metabolic stress. This could reveal the vulnerability of different populations, i.e. pyramidal cells or inhibitory interneurons.

In this study, rat organotypic hippocampal slice cultures, OHSC, (Gähwiler et al., 1997; Noraberg et al., 2005; Schneider et al., 2015) and mouse acute hippocampal slices (Lein et al., 2011) were used as in situ models. The methods applied included: local field potential, LFP, (Einevoll et al., 2013), calcium imaging (Chen et al., 2013; Grienberger and Konnerth, 2012; Kwan, 2008; Podor et al., 2015), oxygen microsensor recordings (Huchzermeyer et al., 2008; Huchzermeyer et al., 2013; Schneider et al., 2017) and spike sorting (Buzsáki and Draguhn, 2004; Quiroga et al., 2004). The combination of the above-mentioned techniques provided us with information about the neuronal network on different temporal and spatial resolutions.

2 Materials and Methods

2.1 Animal preparation

C57BL/6 Mice and Wistar rats were purchased from Charles-River (Sulzfeld, Germany). Caring and sacrificing of the animals were performed according to the recommendations of the European directive (2010/63/EU) and the authorities of Baden-Württemberg (T96/15 and T45/18).

2.2 Organotypic slice cultures

Hippocampal slice cultures were prepared as described earlier (Kann et al., 2003a,b, 2011). Briefly, rats were sacrificed at the age of 7 to 9 days. Under sterile conditions, a McIlwain tissue chopper (Mickle Laboratory Engineering Company Ltd., Guildford, UK) was used to cut hippocampal slices ($\sim$400 µm). The slices were then maintained on Biopore™ membranes (Millicell standing inserts, Merck Millipore, Schwalbach, Germany).

Exchange of culture medium (1 ml) was performed three times per week. The culture medium is composed of 50% minimal essential medium, 25% Hank's balanced salt solution (Sigma-Aldrich, Taufkirchen, Germany), 25% horse serum (Life Technologies, Darmstadt, Germany) and 2 mM L-glutamine (Life Technologies). Slices were kept in a humidified atmosphere (5% CO_2, 36.5°C) in an incubator (Heracell, Thermo Scientific, Dreiech, Germany), and pH was maintained at 7.3. *Organotypic hippocampal slice cultures were prepared by Andrea Lewen.*

2.3 Acute slice preparation

Male C57BL/6 mice (p29-34) were anesthetized using Isoflurane Vapor 19.3 (Dräger, Lübeck, Germany) and laughing gas (70% N_2O and 30% O_2) then decapitated. The brain was quickly extracted and maintained in pre-cooled ($\sim$4 °C) artificial cerebrospinal fluid (ACSF), saturated with 95% O_2 and 5% CO_2. Hippocampal slices were cut horizontally into 400 µm slices using VT 1000s vibratome (Leica, Bensheim, Germany). Then stored in a Haas-type interface chamber at 34 ± 1 °C for 2 h (recovery). The gas supply to the interface chamber was 1.5 l/min (95% O_2 and 5% CO_2).

2.4 Solutions and drugs

Slice cultures / acute slices were constantly supplied with ACSF that contained: 129 mM NaCl, 3 mM KCl, 1.25 mM NaH_2PO_4, 1.8 mM $MgSO_4$, 1.6 mM $CaCl_2$, 21 mM $NaHCO_3$ and 10 mM glucose. A gas mixture of 95% O_2 and 5% CO_2 was used to saturate the recording solution and the pH was 7.4. For ACSF used in the submerged chamber, the concentration of $NaHCO_3$ was increased to 26 mM (see calcium imaging below).

Gamma oscillations were induced (for spike sorting and calcium imaging, see below) by constant bath application of cholinergic receptor agonist, carbachol (20 µM and 10 µM in the interface and submerged chambers, respectively).

Gamma oscillations were also induced for oxygen concentration recordings (see below) using cholinergic agonist, acetylcholine (8 µM) and acetylcholine esterase inhibitor, physostigmine (2 µM) or kainic acid (100 nM; glutamatergic model) in acute slices. In cultures, acetylcholine and physostigmine were used at 2 µM and 0.4 µM, respectively.

Drugs mixture used to block neuronal activity (for oxygen concentration recordings, see below) includes tetrodotoxin (TTX, fast voltage-gated Na^+-channels blocker), DNQX (Selective non-NMDA receptor antagonist), DL-AP5 (selective NMDA antagonist), and atropine (cholinergic receptor antagonist).

Salts, acetylcholine, carbachol, rotenone, and atropine were purchased from Sigma-Aldrich, Germany. TTX and kainic acid from Biotrend, Cologne, Germany. DNQX, DL-AP5 and physostigmine from Tocris (R&D Systems GmbH, Wiesbaden-Nordenstadt, Germany).

2.5 Electrophysiology

Experiments were conducted at 9-10 days *in vitro* (DIV) for recordings for spike sorting and at 4-5 weeks for calcium imaging if not otherwise stated.

Intact Biopore™ membranes were inserted into the interface chamber (spike sorting and oxygen concentration recordings; see below), and supplied with pre-warmed ACSF at 34 ± 1°C. Cut Biopore™ membranes (with Vannas-Tübingen Spring scissor; 15008-08, Fine Science Tools GmbH,

Heidelberg, Germany) were inserted in the submerged chamber for calcium imaging. Recording solution was pre-warmed at 32 ± 1°C. The flow of ACSF was 1.5 - 1.8 ml/min in the interface chamber and 8 ml/min in the submerged chamber. The ambient gas mixture in the interface chamber (95% O_2 and 5% CO_2) was supplied at a flow rate of 1.5 l/min.

Glass electrodes were made from GB150F-8P borosilicate filaments (Science Products GmbH, Hofheim, Germany) for LFP, and from GC120F-10 borosilicate filaments (Clark Electromedical Instruments, Reading, UK) for juxtacellular recording electrodes. Electrodes (tip diameter 3 - 5 µm for LFP recordings and 1.5 µm juxtacellular recordings) were pulled using Zeitz DMZ Puller (Zeitz-Instruments Vertriebs GmbH; Martinsried, Germany) and filled with recording solution. Mechanical micromanipulators (MX-4, Narishige International Ltd, London, UK) aided the positioning of electrodes in the targeted regions for recording. Recordings were performed using an EXT 10-2F amplifier in EPMS-07 housing (npi electronic GmbH, Tamm, Germany). Recordings were low-pass filtered at 3 kHz and digitized at 10 kHz and 20 kHz (LFP, juxtacellular recordings, respectively) using CED 1401 interface and Spike2 software (Cambridge Electronic Design, Cambridge, UK) for storage of data on a computer disk for offline analysis.

We performed spike sorting on recordings with metal electrodes made from 12.5 µm tungsten wire (California Fine Wire Company, Grover Beach, CA, USA) in the interface chamber. Here, an EXT-T1M amplifier was used (npi electronic GmbH, Tamm, Germany). Recordings were low-pass filtered at 3 kHz and digitized at 20 kHz using CED Power3 1401 interface (Cambridge Electronic Design, Cambridge, UK).

2.6 Metabolic stress using different oxygen fractions

Combinations of low oxygen fractions (10%, 5%, and 2%) with standard (10 mM) and reduced (5 mM) glucose concentrations were used to induce different levels of metabolic stress in slice cultures.

The experimental protocol involved recording baseline gamma oscillations (in 95% oxygen fraction) for 10 minutes after having a stable recording. This was followed by a switch to a lower

oxygen fraction (10%, 5% or 2%) for 15 minutes, then further 10 minutes of recovery were oxygen fraction was switched back to 95%.

Five different combinations were tested. Two oxygen fractions (10% and 5%) with standard glucose concentration (10 mM), and three (10%, 5% and 2%) with reduced glucose concentration (5 mM).

2.7 Calcium imaging

Slice cultures were infected with adeno-associated virus (AAV) obtained from Penn Vector Core (Philadelphia, PA, USA) encoding GCaMP6f under the control of the CaMKII promoter (AAV5.CamKII.GCaMPf.WPRE.SV40, Lot # V5392MI-S). AAV transduction was achieved, under sterile conditions, by applying 0.8 µl of the viral particles solution (qTiter: 1.55e13 GC/ml) on top of the slices.

Imaging of the hippocampal CA3 region (with 20x magnification) was performed at 4-5 weeks *in vitro* (3-4 weeks post-viral infection), if not otherwise stated. Slices were maintained in the submerged chamber of Olympus BX51WI microscope (Olympus, Hamburg, Germany). GCaMP6f was excited at 485 ± 10 nm. Fluorescence images (emission at 521 ± 10 nm) were recorded at 4 Hz using a CCD camera (ORCA-ER; Hamamatsu Photonics, Hamamatsu City, Japan).

Before transferring slice cultures to the submerged chamber (10 µM carbachol) for imaging, persistent gamma oscillations were induced in the interface chamber (20 µM carbachol). Imaging was performed for 5 minutes during baseline gamma oscillations. Rotenone was then applied and after ~ 5 minutes imaging was resumed for an additional 5 minutes during the mild metabolic stress condition.

2.8 Ensembles detection

Fluorescent traces were obtained from raw pixel values from manually-drawn regions of interest (ROI) using Fiji (Schindelin et al., 2012). A custom-made algorithm (Matlab 2018b, MathWorks, Natick, MA, USA) algorithm was used to calculate average fluorescent signal from pixels within ROIs that reported true signal after discarding pixels reporting cross-talk contamination. A

standard deviation projection for the full acquisition time is constructed. The darkest 5% of the total area of the hippocampal tissue was considered a background. After background subtraction, F/F_0 was calculated by comparing the maximum value (F) during an event to baseline directly before the event (F_0).

For a true signal to be detected (Figure 11A), two conditions have to be satisfied. First, traces from all pixels within the relevant ROI should show higher values (at least 95% of the pixels) than the baseline fit of the traces. This indicates that the whole ROI is fluorescing which occurs if a cell is active. However, out of focus background can increase pixel values in the ROI as well, leading to false positive signal. Therefore, the second condition is that the average pixel values from the surrounding region (border of the ROI) is lower than the values of pixel within the ROI (less than the lowest 5%).

On the contrary, when contamination of the complete ROI occurs (Figure 11B), transients from the surrounding region are high enough relative to values of pixels within the ROI (higher than the lowest 5%), thereby, violating the second condition described above. In this case, the difference between activity outside and within the ROI during the events was linearly interpolated between the beginning and end of the relevant event. In the case of partial overlap contamination (Figure 11C), violation of the first condition occurs, in which only a portion of pixels show elevated transients. These pixels are clustered using K-means and their fluorescent transients are discarded from calculating the final average fluorescent signal. The ratio between the highest and lowest 5% of pixel values for every time point is used to detect such false events. If the ratio during an event is higher than 95% of ratio values calculated for the full acquisition time, the event is a result of partial contamination of the relevant ROI and is labeled as a false event.

For detection of synchronized activity, fluorescence transients were smoothed by sliding average window of 1s. The preprocessed calcium traces were analyzed as described before (Hamm et al., 2017). Briefly, the method depends on bootstrapping which is applied to identify above-chance population activity, producing population vectors as an output. The vectors are then filtered based on their similarity indices to yield only 'repetitive' above-chance activity. Afterwards, calcium transients were translated to binary output in which recruited cells at the time points of

synchronized activity were translated to ones (Figure 13A). The output is population vectors in binary code. These vectors were then categorized by principal component analysis followed by clustering using Fuzzy C-means and Dunn's index (Sasaki et al., 2007) into ensembles of pyramidal cells (Figure 13B).

2.9 Oxygen concentration recordings

Oxygen recordings were performed using Clark-type oxygen microsensor, OX-10 (Unisense, Aarhus, Denmark) connected to a 4-channel Microsensor Multimeter (Unisense). The spatial resolution of O_2-sensor at the tip diameter is 8–12mm. The O_2-sensor was polarised with 800 mV overnight. Calibration is performed before and between experiments using a two-point calibration, by ACSF (salinity 11%) which was saturated with 0% O_2 (0% O_2 and 100% N_2) and 95% O_2 (95% O_2 and 5% CO_2) at 34 °C. Oxygen depth profiles were measured in CA3 *stratum pyramidale* in cholinergic and glutamatergic gamma models. In another set of experiments, profiles were measured in CA3 *stratum pyramidale* and *stratum radiatum* simultaneously in glutamatergic gamma model. The profile measurements were performed starting at tissue surface and further steps of ~20 µm along vertical axis until oxygen concentration increased again due to supply from beneath the tissue (recording solution). Wash of TTX (0.5 µM), atropine (1 µM), DNQX (10 µM) and DL-AP5 (50 µM) followed oxygen depth profiles of cholinergic and glutamatergic models (in *stratum pyramidale*), to block neuronal activity and serve as a reference. Oxygen concentrations were used in a mathematical reaction-diffusion model to estimate the local $CMRO_2$ in a tissue volume of 1 x 10^5 to 2.25 x 10^5 mm^3 [V = (d/2)^2 x π x L, with d corresponding to the tip diameter of the O_2-sensor, and L corresponding to the mean tissue depth of 199.2 mm]. The oxygen concentration in ACSF saturated with 95% O_2 at 34 °C was 941 mM. The corresponding oxygen partial pressure (pO_2) was 684.3 mmHg (pO_2 = (p$_{atm}$ - p$_{vapor}$) x 95%), with atmospheric pressure, p$_{atm}$ = 760 mmHg and water vapor pressure, p$_{vapor}$ = 39.7 mmHg at 34 °C. Thus, the factor to convert µM to mmHg was 0.73 mmHg/µM. *Calculations of cerebral metabolic rates were performed by Dr. Nikolaus Berndt.*

2.10 Data analysis

Analysis of the electrophysiological signals was accomplished off-line using Spike2 and Matlab. LFP signals of 5 min were subdivided into segments of 30 s, band-pass filtered (fast Fourier transform, FFT, pass-band frequency: 5 - 200 Hz, 8th order) and processed with Welch's algorithm and a fast Fourier transformation (FFT size: 8192). Gamma oscillations were analyzed for peak frequencies, peak power, full width at half-maximum (FWHM) and area under the curve (AuC) of power spectra using custom-made Matlab algorithms. FWHM reflects the synchrony of activated synapses. The direction of gamma oscillations propagation was determined by performing cross-correlation analysis which detects time lag between signals recorded from different regions in the hippocampus. Spike sorting was performed using Wave_Clus (Quiroga et al., 2004). Parameters used for analysis are provided in Table 1. We categorized sorted units according to their firing rates during baseline gamma oscillations. Based on our juxtacellular recordings and a previous study (Csicsvari et al., 1999; Zemankovics et al., 2013), we set a threshold of 10 Hz for FSUs, and 5 Hz for SSUs.

Data are collected from 'n'; the number of slices prepared from 'N'; the number of animals or preparations. Data are summarized by their median ± the interquartile range (IQR = 75% percentile - 25% percentile), error bars indicate minimal and maximal values. Figures were generated using CorelDRAW X7 (Corel, Ottawa, Canada).

2.11 Statistical evaluation

Statistical analysis was performed using Prism 6 (GraphPad, CA, USA). Shapiro-Wilk test was used to test for normality in the data distribution. Comparisons among paired data were made with paired *t*-test (two groups) or repeated measures ANOVA with Holm-Sidak's multiple comparisons test (more than two groups) if normally distributed, otherwise Wilcoxon signed-rank test (two groups) or Friedman with Dunn's multiple comparison test (more than two groups). Comparisons among unpaired data were made with unpaired *t*-test (two groups) or one-way ANOVA with Holm-Sidak's multiple comparisons test (more than two groups) if normally distributed, otherwise Mann-Whitney test (two groups) or Kruskal-Wallis with Dunn's multiple comparisons test (more than two groups). To test for correlations, the correlation coefficient *r* and *p*-values were

computed using the Pearson correlation. *p*-values less than 0.05 (indicated by asterisks) were considered to indicate a significant difference between compared groups. To test the difference between the cumulative distribution functions, we used two-sample Kolmogorov-Smirnov test.

Table 1 Parameters used in Wave_Clus, the spike sorting Matlab algorithm.

`par.segments_length`	5
`par.sr`	20000
`par.cont_segment`	true
`par.max spikes plot`	1000
`par.print2file`	true
`par.cont plot samples`	100000
`par.to plot std`	1
`par.all_classes_ax`	'mean'
`par.plot_feature_stats`	false
`par.mintemp`	0.00
`par.maxtemp`	0.251
`par.tempstep`	0.01
`par.SWCycles`	100
`par.KNearNeighb`	11
`par.min_clus`	20
`par.max_clus`	200
`par.randomseed`	0
`par.temp_plot`	'log'
`par.c_ov`	0.7
`par.elbow min`	0.4
`par.tmax`	'all'
`par.tmin`	0
`par.w pre`	20
`par.w_post`	44
`par.alignment_window`	10
`par.stdmin`	5
`par.stdmax`	50
`par.detect_fmin`	300
`par.detect_fmax`	3000
`par.detect_order`	4
`par.sort_fmin`	300
`par.sort_fmax`	3000
`par.sort_order`	2
`par.ref ms`	1.5
`par.detection`	'neg'
`par.int_factor`	5
`par.interpolation`	'y'
`par.min_inputs`	10
`par.max_inputs`	0.75
`par.scales`	4
`par.features`	'wav'
`par.template_sdnum`	3
`par.template_k`	10
`par.template_k_min`	10
`par.template_type`	'center'
`par.force_feature`	'spk'
`par.force_auto`	false
`par.match`	'n'
`par.max_spk`	4000000
`par.permut`	'n'
`par.nbins`	100
`par.bin_step`	1

3 Results

3.1 Validation of OHSCs for studying neuronal networks

In a set of experiments, we performed simultaneous LFP recordings using four electrodes. Gamma oscillations were induced by constant bath application of acetylcholine (2 μM) and physostigmine (400 nM) in the interface chamber. The oscillations were recorded from four different regions of the hippocampus, i.e. dentate gyrus (DG), proximal CA3, distal CA3 and CA1 (Figure 3). Similar patterns of activity were observed in the different examined locations, indicating that a specific activity state is present globally across a large portion of the hippocampus rather than being restricted to a specific region.

Additionally, we determined the propagation direction of gamma oscillations by performing cross-correlation analysis. Signals from DG, distal CA3 and CA1 were observed to lag the signals from the proximal CA3, therefore proximal CA3 was used as a reference. The time shifts between proximal CA3 and signals from DG, distal CA3, and CA1 were 0.48 ± 0.12 ms, 0.28 ± 0.13 ms and 1.39 ± 0.20 ms, respectively (n=11, N=4).

Besides, in another set of experiments, simultaneous LFP recordings in *stratum pyramidale* and *stratum radiatum* showed a reversal in the signal potential. This complies with known current source densities in previous studies (Hájos and Paulsen, 2009; Vodovozov et al., 2018).

3.2 Induction of mild metabolic stress

3.2.1 Metabolic stress using different oxygen fractions

Here, we determined the combination of oxygen fraction and glucose concentration that induces a controllable metabolic stress condition. We used OHSCs in the interface chamber and induced gamma oscillations by constant application of acetylcholine (2 μM) and physostigmine (400 nM).

Three phases were analyzed for comparison, baseline reflecting stable gamma oscillations in 95% oxygen fraction, followed by hypoxia for 15 minutes and finally recovery, were oxygen fraction is switched back to 95%.
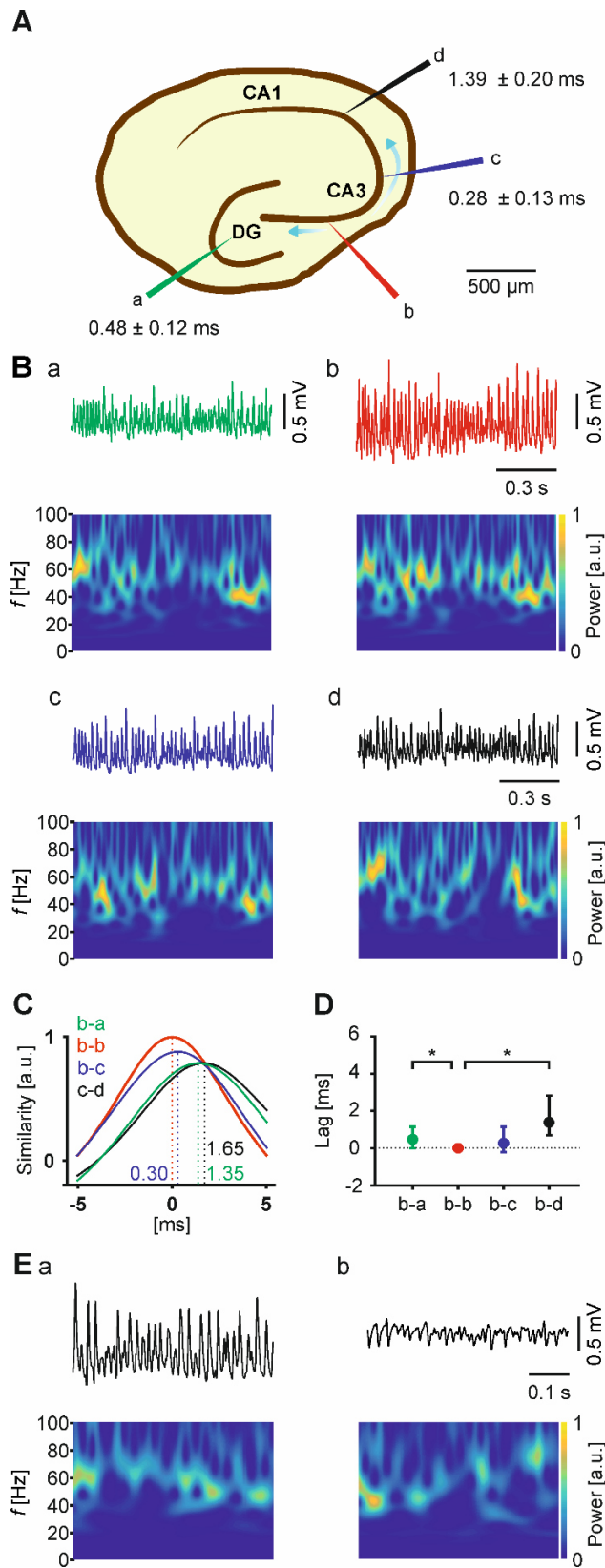
Figure 3. Characteristics of gamma oscillations in different regions of the hippocampus. A, Diagram of the hippocampus and the regions where simultaneous recordings were performed. Times represent the lag (mean ± SEM) between different regions in reference to proximal CA3 (electrode 'b'). **B**a-d, Example traces of gamma oscillations from different regions as indicated in **A** (n=11, N=4). LFP traces are presented (top) with corresponding wavelet transformations (bottom) showing the power of frequency domains over time. Heat-scale colors encode for power in arbitrary units (a.u). **C**, Cross-correlation of representative traces. The red curve represents the autocorrelation of proximal CA3 recording (electrode 'b' in A). In blue, recording from distal CA3 (electrode 'c') is cross-correlated to proximal CA3 (electrode 'b'). In green, recording from the dentate gyrus (electrode 'a') is cross-correlated to proximal CA3 (electrode 'b') trace from. In black, recording from CA1 (electrode 'd') is cross-correlated to proximal CA3 (electrode 'b'). **D**, Lag between different regions. Comparison of cross-correlations from different regions (b-a, b-c, and b-d) was performed in relation to the location of electrode 'b' (b-b). Values indicate mean and range. Friedman test was performed, followed by Dunn's multiple comparison test. **E**, Sample traces of gamma oscillations recorded simultaneously in stratum pyramidale (a) and stratum radiatum (b) in CA3. Corresponding wavelet transformations (bottom) show the power of frequency domains over time. Heat-scale colors encode for power in arbitrary units (a.u). * p < 0.05

25

Hypoxia included 10%, 5% or 2% oxygen fraction. Glucose concentration was fixed during the three phases, either standard (10 mM) or reduced (5 mM). See 2.6 in Materials and Methods for the applied combinations.

Time series (Figure 4) show the changes in frequency and power during the three phases for all tested combinations. It is noted that the reductions in power occur rapidly after switching to hypoxia and the ongoing dynamic phase lasts only for a short period.

The parameters analyzed for gamma oscillations include frequency, power, FWHM and AuC (Figure 5). It is observed that power showed significant changes in combinations of low oxygen fraction and reduced glucose concentration (5 mM). Interestingly, FWHM showed significant changes only with 5% and 2% oxygen fractions. Since FWHM reflects synchrony, we further investigated if the effects on power or FWHM result from low glucose concentration or oxygen fraction, respectively.

To isolate the effect of glucose concentration, we pooled measures of baseline power from recordings with 10 mM glucose and compared them to recordings with 5 mM glucose. Surprisingly, neither power nor FWHM was changed (Figure 6).

Following, we isolated the effect of changing oxygen fractions. Dose-response curves in standard glucose concentration showed no changes in power nor in FWHM (Figure 7A). However, in reduced concentration (Figure 7B), significant changes were observed in all calculated parameters.

These results showed that the available durations for analysis upon induction of metabolic stress are short for implementing a robust analysis. Therefore, we examined a different approach (pharmacological) for inducing stress, which is the application of rotenone (inhibitor of complex I of the electron transport chain).
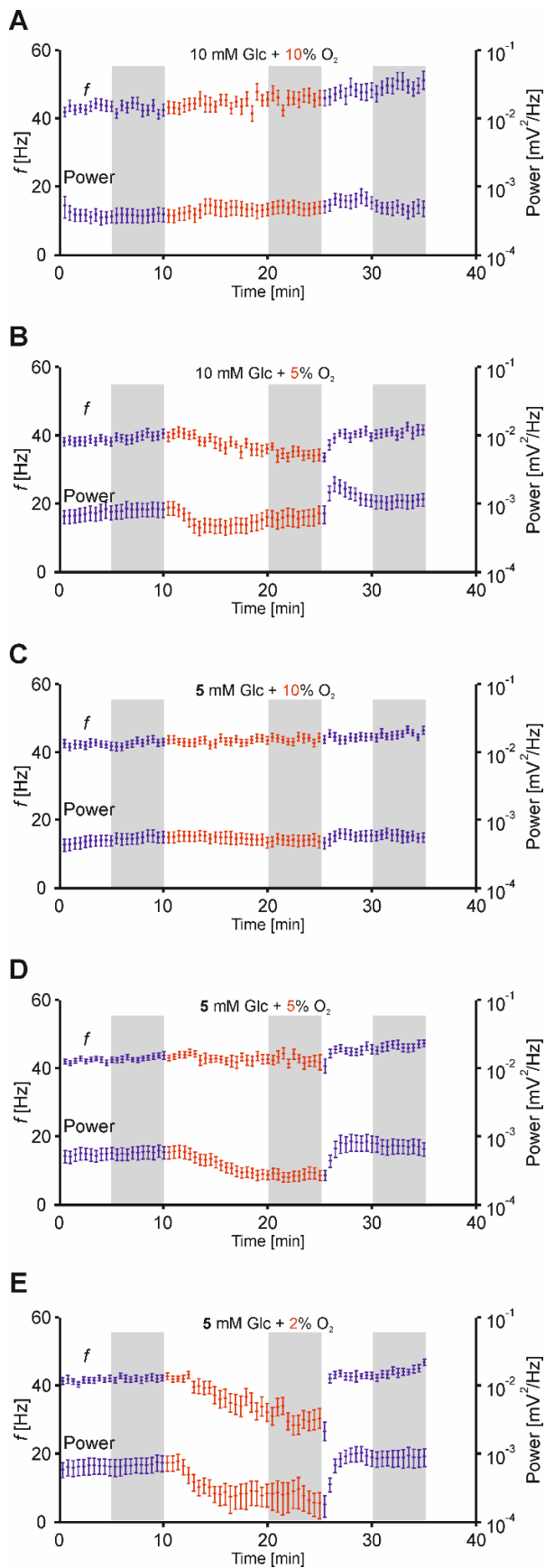
Figure 4. Metabolic stress combinations of hypoxia and glucose (Glc) concentration. A-E, Time series for frequency (*f*) and peak power spectral density (Power). Grey rectangles highlight periods of comparisons between baseline, hypoxia, and recovery. Glc concentrations (top) were used during the whole recording. Oxygen concentration (in red, hypoxia) was used only during hypoxia. n/N slices/preparations: **A** 21/4; **B** 21/3; **C** 18/3; **D** 29/3; **E** 29/3.
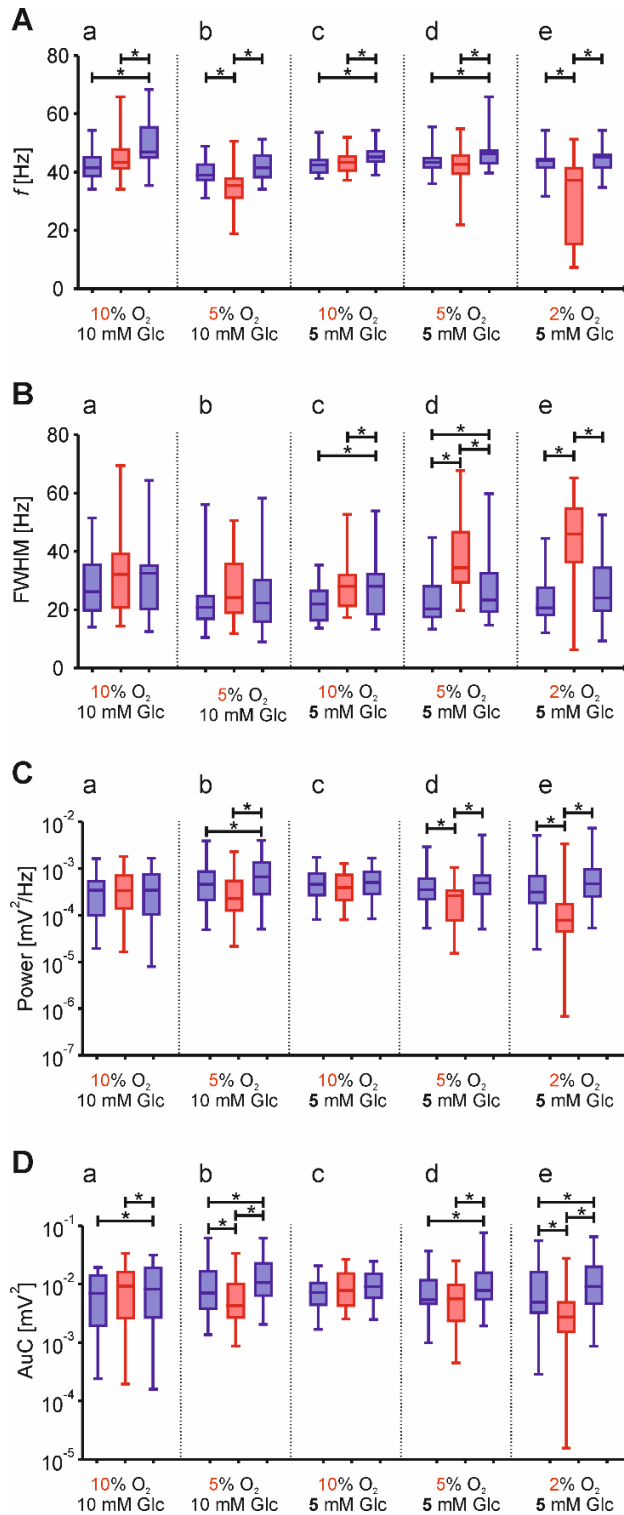
Figure 5. Synopsis of metabolic stress combinations of hypoxia and glucose (Glc) concentration. Gamma oscillations were analyzed for different parameters. Comparisons between baseline, hypoxia, and recovery. n/N slices/preparations in **A-D**: **a** 21/4; **b** 21/3; **c** 18/3; **d** 29/3; **e** 29/3. **A**, Peak frequency (*f*). **Aa**, Friedman with Dunn's multiple comparison test. **Ab**, one-way ANOVA with Holm-Sidak's multiple comparisons test. **Ac-e**, Friedman with Dunn's multiple comparison test. **B**, Full width at half-maximum (FWHM). **Ba**, one-way ANOVA with Holm-Sidak's multiple comparisons test. **Bb-e**, Friedman with Dunn's multiple comparison test. **C**, Peak of power spectral density (Power). **D**, Area under the curve (AuC). **C-D** Friedman with Dunn's multiple comparison test. * p < 0.05. Data are summarized by their median ± the interquartile range (IQR = 75% percentile - 25% percentile), error bars indicate minimal and maximal values.
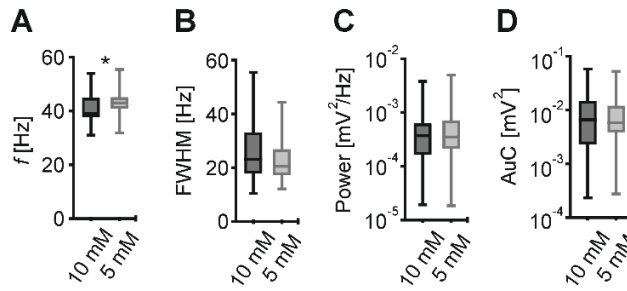
Figure 6. Isolated effect of glucose on gamma oscillations. Gamma oscillations were analyzed for different parameters. n/N slices/preparations in **A-D**: 42/6 pooled for 10 mM glucose, 76/6 pooled for 5 mM glucose. **A**, Peak frequency (*f*). **B**, Full width at half-maximum (FWHM). **C**, Peak of power spectral density (Power). **D**, Area under the curve (AuC). **A-D**, Mann-Whitney test. * p < 0.05. Data are summarized by their median ± the interquartile range (IQR = 75% percentile - 25% percentile), error bars indicate minimal and maximal values.
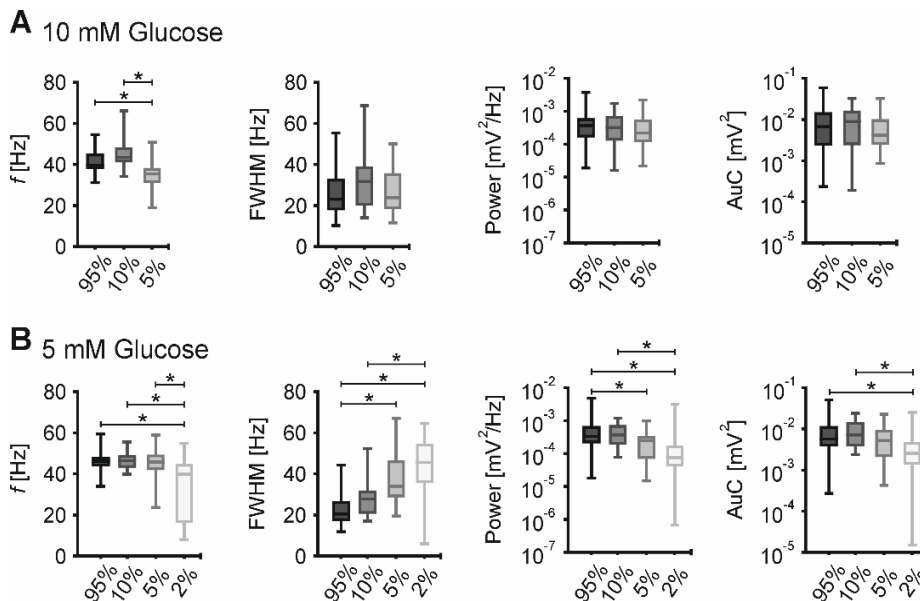
Figure 7. Dose response of different oxygen fractions. Gamma oscillations were analyzed for different parameters (Frequency, FWHM, Power, and AuC) in standard (**A**) and reduced (**B**) glucose concentrations. n/N slices/preparations in **A**: 42/6 pooled for 95% O_2, 21/4 for 10% O_2 and 21/3 pooled for 5% O_2. n/N in **B**: 76/6 pooled for 95% O_2, 18/3 for 10% O_2, 29/3 for 5% O_2 and 29/3 for 2% O_2. **A-B**, Kruskal-Wallis with Dunn's multiple comparisons test. * p < 0.05. Data are summarized by their median ± the interquartile range (IQR = 75% percentile - 25% percentile), error bars indicate minimal and maximal values.

3.2.2 Gamma oscillations in submerged condition

In this set of experiments, cultures were maintained for at least 25 minutes in an interface chamber to induce gamma oscillations in optimal conditions. Carbachol was used at 20 µM in the interface chamber. Following, cultures were transferred to the submerged chamber, where 10 µM of carbachol was used.

The carbachol concentration, temperature and flow rate were sufficient for inducing persistent gamma oscillations in the slices (Figure 8). The oscillations lasted stably for more than 25 minutes in the submerged chamber without any significant changes in the measured parameters; frequency, power, FWHM, and AuC.

The stable duration of gamma oscillations is considered satisfactory for performing imaging with OHSCs in submerged conditions. Thereby, the activity of a large number of cells can be monitored simultaneously.
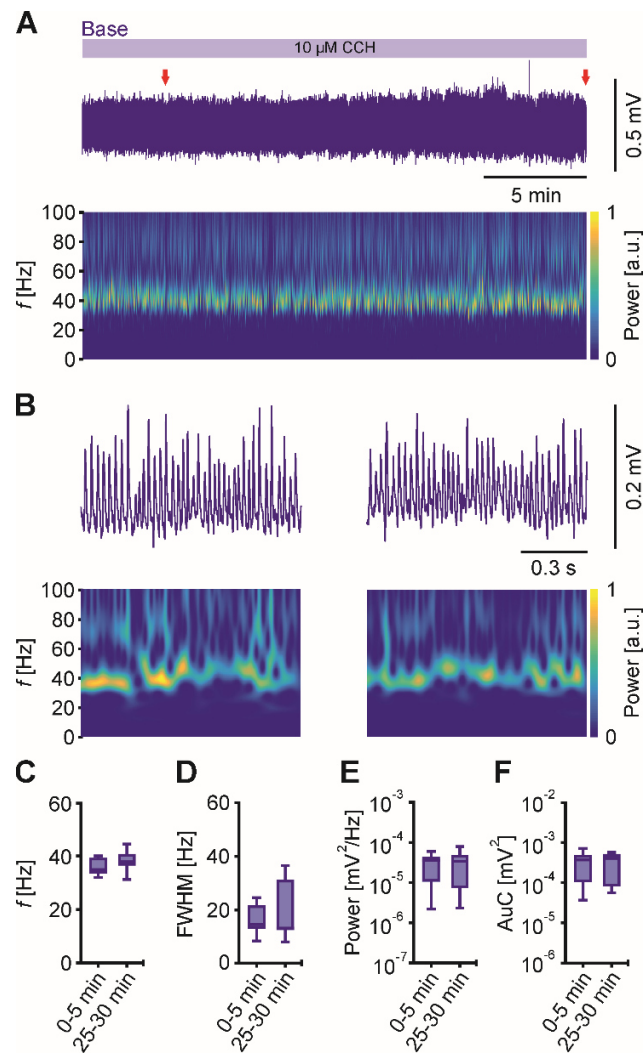
Figure 8. Stable gamma oscillations can be induced persistently in submerged condition. A, Sample trace of LFP recording during gamma oscillation (top). Red arrows indicate time points in **B** at higher temporal resolution. Corresponding wavelet transformations (bottom) showing the power of frequency domains over time. Heat-scale colors encode for power in arbitrary units (a.u.). Gamma oscillations were analyzed for different parameters for the first and last 5 minutes of the recordings. n/N slices/preparations: 7/2. **C**, Peak frequency (*f*), paired t-test. **D**, Full width at half-maximum (FWHM), Wilcoxon matched-pairs signed-rank test. **E**, Peak of power spectral density (Power), paired *t*-test. **F**, Area under the curve (AuC), paired *t*-test. This experiment was conducted within 2-3 weeks *in vitro*. Data are summarized by their median ± the interquartile range (IQR = 75% percentile - 25% percentile), error bars indicate minimal and maximal values.

31

3.2.3 Metabolic stress using rotenone

In order to challenge the coordinated activity of the neuronal network, we applied rotenone at a low concentration (0.1 µM). The resulting partial block of the electron transport chain lowers the mitochondrial ATP production and finally leads to metabolic stress. Application of rotenone affected the network only mildly; no significant changes in frequency or FWHM were detected (Figure 9C-D). However, power and AuC were significantly reduced (Figure 9E-F). At the induced stress level we did not observe any pathologic activity in the LFP (wavelet spectra in Figure 9).

It is observed that during the application of rotenone the changes were dynamic (Figure 9A top right). Therefore, we further analyzed the ongoing decay of gamma oscillations during metabolic stress to exclude the loss of gamma oscillations during the application of rotenone (Figure 10). Although power and AuC were significantly reduced, the network activity itself was still in the gamma range.

Our data show that the low concentration of rotenone causes mild metabolic stress which attenuates the gamma oscillations on the network level. But the effects on the cellular level were still to be examined. Therefore, we performed calcium imaging to record changes in the activity of pyramidal cells under metabolic stress conditions.
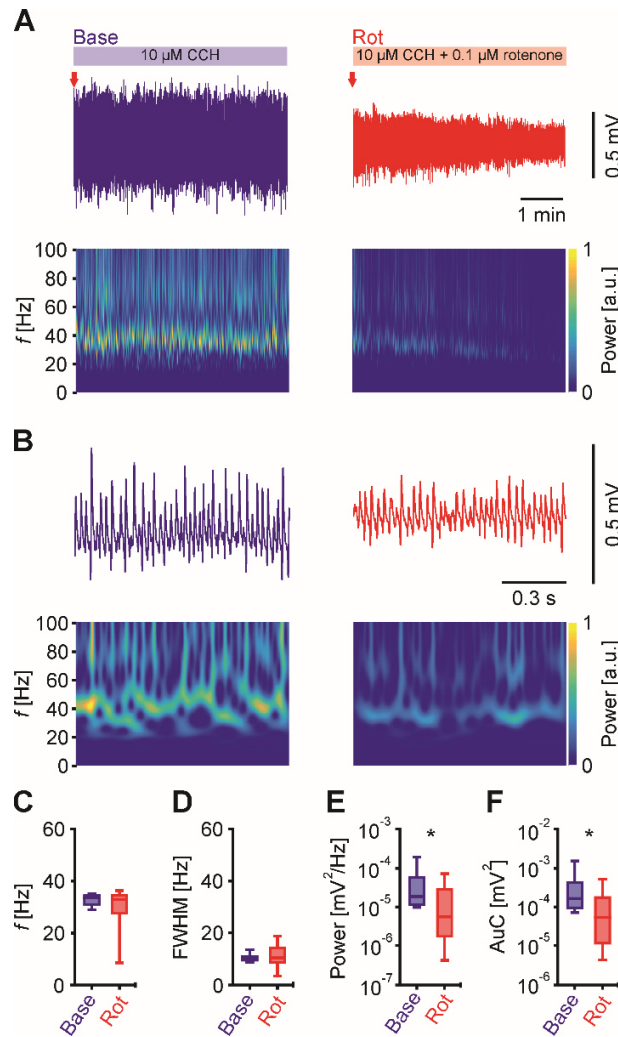
Figure 9. Gamma oscillations challenged by mild metabolic stress using rotenone. Local field potentials were recorded in submerged condition. **A**, Sample traces of cholinergically induced gamma oscillations (blue, top left) and during additional application of rotenone (0.1 μM, red, top right). Red arrows indicate time points in **B** at higher temporal resolution. Corresponding wavelet transformations (bottom) showing the power of frequency domains over time. Heat-scale colors encode for power in arbitrary units (a.u.). Note that wavelet transformations during rotenone application are normalized to transformations during baseline. Gamma oscillations were analyzed for different parameters for the shown duration of baseline and rotenone application in **A**. n/N slices/preparations: 8/3. **C**, Peak frequency (*f*), Wilcoxon matched-pairs signed-rank test. **D**, Full width at half-maximum (FWHM), paired t-test. **E**, Peak of power spectral density (Power), Wilcoxon matched-pairs signed-rank test. **F**, Area under the curve (AuC), Wilcoxon matched-pairs signed-rank test. * *p* < 0.05. Data are summarized by their median ± the interquartile range (IQR = 75% percentile - 25% percentile), error bars indicate minimal and maximal values.
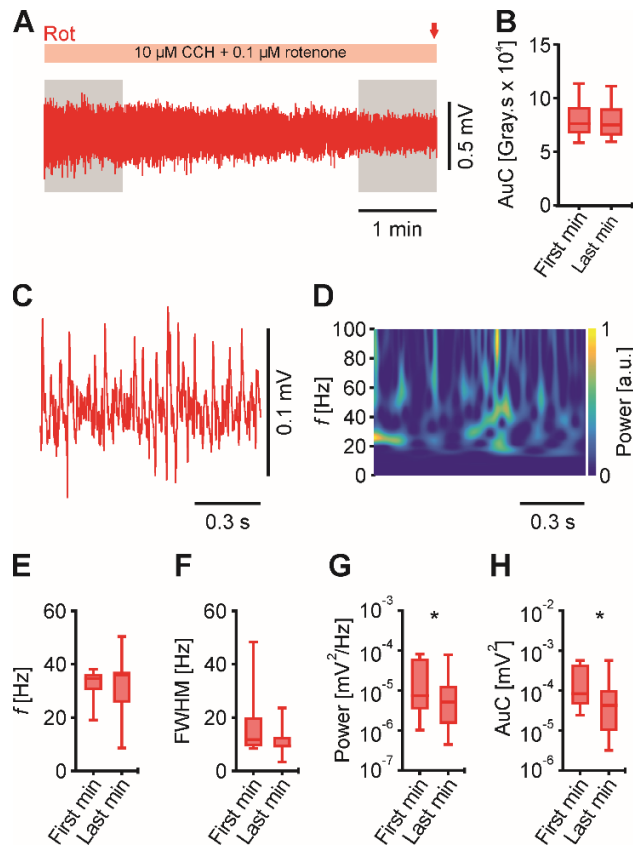
Figure 10. Metabolic stress induced by rotenone is dynamic but mild. A, Sample trace of LFP recording during mild metabolic stress. Gray rectangles (one minute each) indicate time windows compared in the following statistics. n/N slices/preparations: 8/3. Red arrows indicate time points in **C** at higher temporal resolution and corresponding wavelet transformations showing the power of frequency domains over time in **D**. **B**, Area under the curve for calcium fluorescence reflecting the overall activity of pyramidal cells, paired t-test. Gamma oscillations were analyzed for different parameters. **E**, Peak frequency (*f*). **F**, Full width at half-maximum (FWHM). **G**, Peak of power spectral density (Power). **H**, Area under the curve (AuC), **E-F**, Wilcoxon matched-pairs signed-rank test. Note the difference between AuC in **B** (calcium fluorescence of pyramidal cells) and AuC in **F** (derived from power spectra of LFP). * $p < 0.05$. Data are summarized by their median ± the interquartile range (IQR = 75% percentile - 25% percentile), error bars indicate minimal and maximal values.

3.3 Challenging pyramidal cell ensembles

3.3.1 Algorithm for minimizing cross-talk

Cross-talk is a common issue in imaging with wide-field microscopes due to overlapping somata of different neurons. We developed a custom-made MATLAB algorithm to reduce contamination in reported calcium transients (see Materials and Methods).

Briefly, 1) a true signal (Figure 11A) is detected when first, the pixel values (within ROI) are above the baseline and second, the average pixel values from surrounding region (border of ROI) is lower than pixel values within the ROI. 2) Complete overlap of ROI with background activity (Figure 11B) is detected when activity from the surrounding region (border) is relatively high to pixel values within the ROI. In this case, the difference between activity outside and within ROI is interpolated linearly between the beginning and end of the event. 3) Partial overlap (Figure 11C) with a neighboring active cell is detected when only a small portion of pixels show elevated transients. These pixels are clustered and their calcium transients are discarded from constructing the final calcium transients.
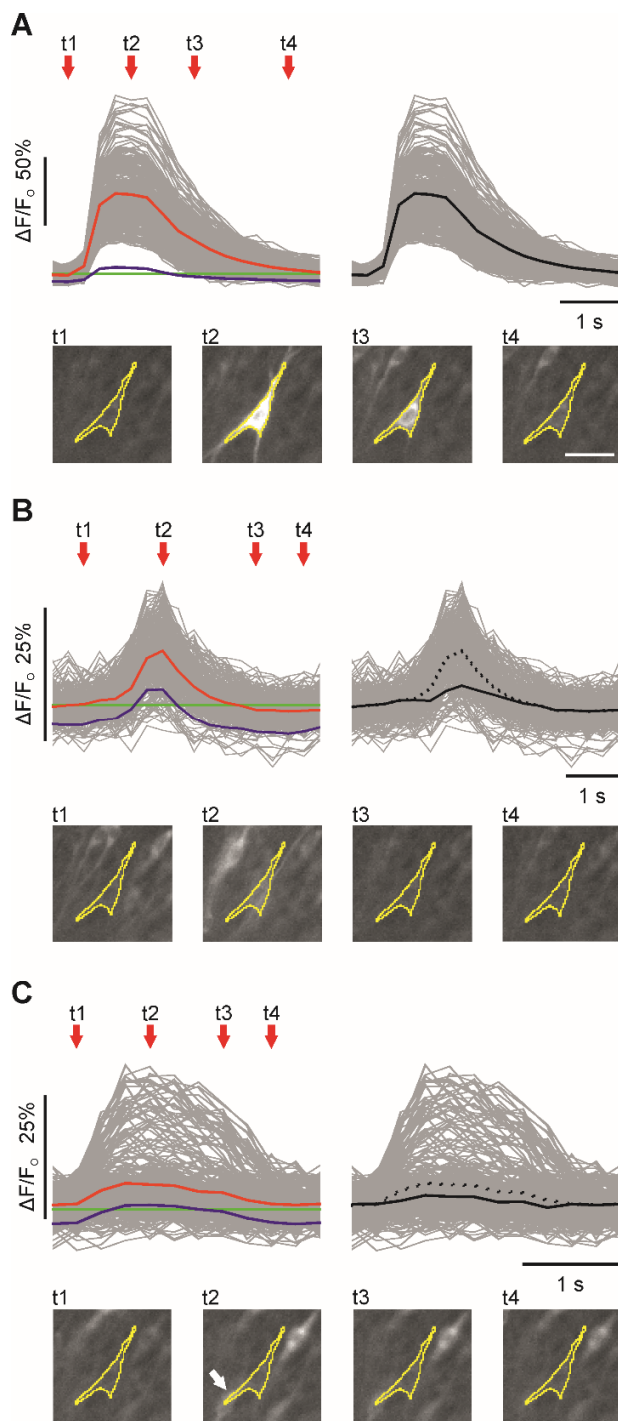
Figure 11. Algorithm for reducing cross contamination of calcium fluorescence signal. Three possible conditions can occur, true signal (**A**), contamination with complete overlap with the region of interest (ROI) because of background activity (**B**), or partial contamination due to overlap with active neighboring cells (**C**). **A**, Light grey traces (top) represent calcium fluorescence transients of all pixels within the ROI marked with yellow (bottom). Red, green and blue traces (top left) represent average calcium fluorescence within ROI, baseline and average calcium fluorescence of ROI's surrounding border, respectively. The black line (top right) shows the output of the algorithm. At the bottom, the four time points are marked with red arrows (top left) indicating that observed signal is a true intrinsic activity of the ROI. **B**, Dashed black line (top right) indicate contaminated signal (equal to the red line, left). The solid black line shows the output of the algorithm. **C**, Note the active neighboring cell (white arrow at 't2', bottom) overlapping with ROI. Scale bar 20 μm.

### 3.3.2 Synchronized activity is more vulnerable than the overall activity.

To monitor the changes at the cellular level, we used GCaMP6f to report the neuronal activity of pyramidal cells. Juxta-cellular recordings show the action potential firings underlying the fluorescent transients during gamma oscillations (Figure 12A-B). The average firing rate of pyramidal cells was 2.18 ± 0.23 Hz (mean ± SEM, 17 cells from 17 slices from 5 preparations). We imaged for five minutes during baseline gamma oscillations and during mild metabolic stress, similar to the experiments shown in Figure 9. In this dataset (8 slices, 3 preparations) we monitored the activity of 50 up to 155 neurons.

The current model (slice cultures in submerged condition) and custom-made algorithms (see Materials and Methods) enabled detecting synchronized, 'above chance', activity. Beginnings of these events are marked with black dots (Figure 12C). The spatial distribution of a subset of these cells (dashed rectangle in Figure 12C) is shown in Figure 12D. The wide distribution of these cells proves the absence of cross-talk and that the observed synchronized activity in Figure 12E (Base) is intrinsic to the network activity underlying gamma oscillations.

Although achieved metabolic stress is mild, however, synchronized activity is clearly perturbed (Figure 12E, Right), indicating their high vulnerability at the current stress level. Figure 12F shows the similarity between events of synchronized activity (black dots in Figure 12C). The similarity is based on comparing the set of contributing cells to these events. The brighter the heat-scale color for any pair of compared events, the more similar is the set of pyramidal cells active during these events. The duration of image acquisition is considered sufficient for robust analysis since we already detected repetitive patterns of synchronized activity (Figure 12F) during baseline gamma oscillations (Figure 12E, left).

To quantify the changes in synchronized activity, we used two measures. First, the percentage of recruited cells, second, the summed duration of synchronized activity (Figure 12G-H). These parameters report the number of cells participated in any synchronized event (black dots in Figure 12C) and the summed duration of these events compared to total acquisition time (5 min). A clear reduction is observed in both measures. Interestingly, the overall activity of pyramidal cells (Figure 12I) reported as AuC of calcium transients showed no change upon mild metabolic stress.

These findings demonstrate that recruiting groups of cells into synchronized patterns of activity is metabolically more demanding than maintaining their overall activity. Following the investigation on the cellular level, we further investigated effects occurring at the ensemble's level.
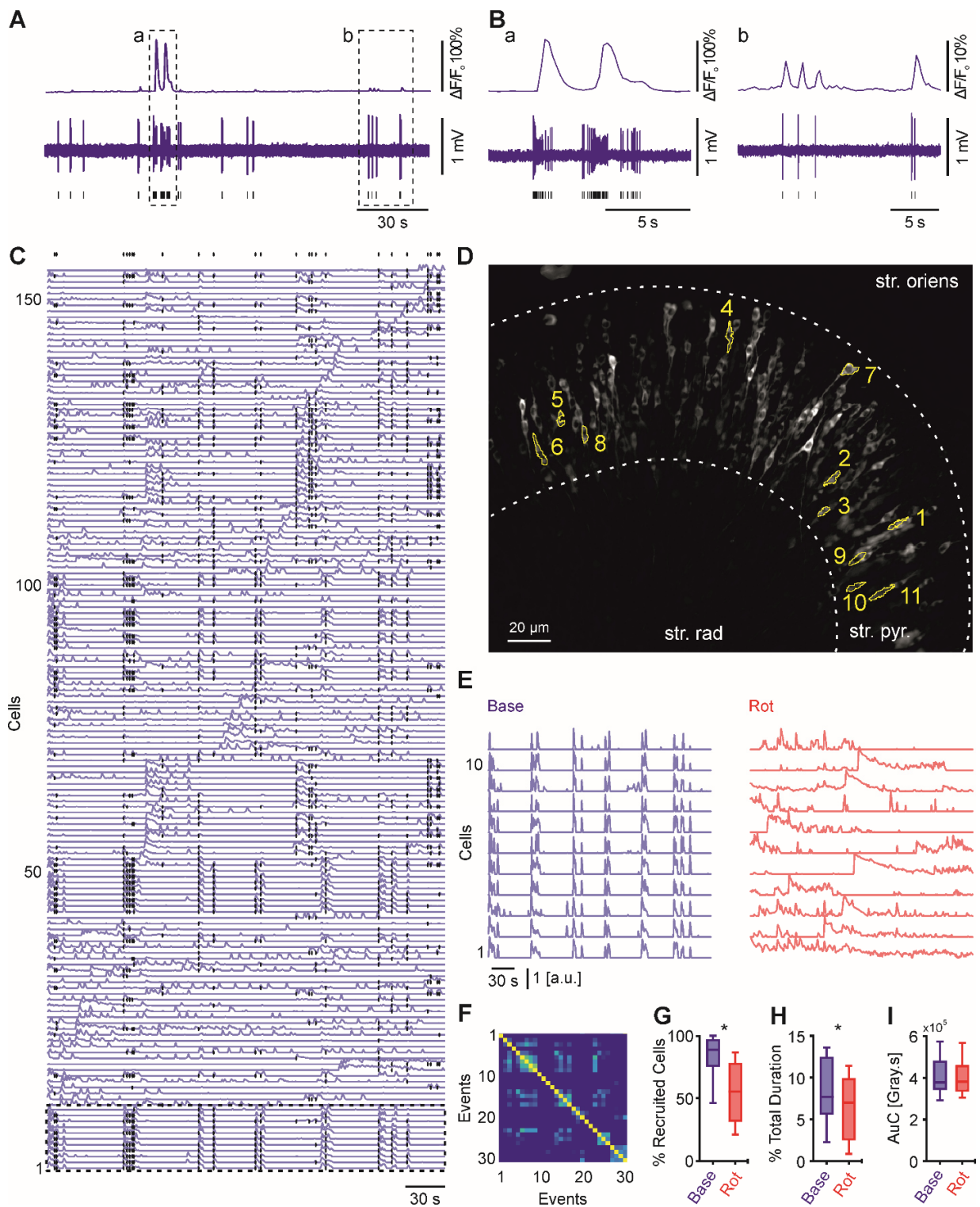
Figure 12. Mild metabolic stress attenuates the synchronized but not the overall activity of pyramidal cells. Calcium fluorescence and simultaneous juxtacellular signals were recorded in submerged condition. **A,** Traces of calcium fluorescence (top) with corresponding cell activity (juxtacellular recording, middle). Black lines indicate times of action potentials fired by recorded cell (bottom), cells/slices/preparations:

17/17/5. Dashed rectangles (**a**-**b**) indicate traces at higher resolution in **Ba**-**b. C,** Traces of calcium fluorescence for all detected cells (n = 155) in one slice. Black dots (top) indicate beginnings of periods of synchronized activity and participating cells. Dashed rectangle (bottom) marks the 11 cells represented in **D-E**. **D,** Standard deviation projection of calcium fluorescence for the whole acquisition time during baseline gamma oscillations (5 min). Note that the highlighted cells elicit synchronized activity (in **E**, left). str. oriens, Stratum oriens; str. pyr., Stratum pyramidale; str. rad., Stratum radiatum. **E,** Highlighted cells in **C-D** show synchronized activity during baseline gamma oscillations (blue, left) while in the presence of rotenone activity shifts to a less synchronized pattern (red, right). **F,** Similarity matrix for events of synchronized activity (marked with black dots in **C**). Note the bright blue spots far from the diagonal. The brighter, the more similar the set of active cells in compared events. This indicates that these set of cells are repetitively active. Synchronized and overall activity were analyzed for different parameters. For cells/slices/preparations: 713/8/3. **G,** Percentage of recruited cells during synchronized activity. **H,** Percentage of the summed duration of the synchronized activity. **I,** Area under the curve (AuC) for calcium fluorescence, reflecting the overall activity of pyramidal cells. **G-I** paired t-test, * $p < 0.05$. Data are summarized by their median ± the interquartile range (IQR = 75% percentile - 25% percentile), error bars indicate minimal and maximal values.

3.3.3   Pyramidal cells are mildly disinhibited and ensembles are disrupted.

To determine the number of pyramidal cell ensembles underlying the synchronized events, we translated calcium transients into a binary output (Sasaki et al., 2007), i.e. calcium transients of active cells during synchronized events are translated to logical 'ones'. The output of this operation is population vectors (Figure 13A-B). These vectors were then differentiated by PCA followed by clustering using Fuzzy C-means and Dunn's index into ensembles of pyramidal cells (Figure 13C-D).

We observed that most of the detected cells are recruited into ensembles. We also investigated whether there is a difference in the number of cells participating only in a single or multiple ensembles. The lack of any significant difference (Figure 13E), indicates that a fixed portion (~ 50%) of the detected cells is recruited in ensembles formation. The number of detected ensembles ranged from one to three per slice (Figure 13F). A total of 17 ensembles from all slices showed an average of 58.5 ± 8.3 constituent cells (mean ± SEM, n = 8 slices from 3 preparations).

To determine whether slices with a low number of active cells hindered ensembles detection, we calculated correlations between the number of cells, events and detected ensembles (Figure 13F-H). The absence of any correlation suggests that the number of detected cells and events reflect the intrinsic activity underlying gamma oscillations and did not hinder the detection of ensembles.

40

We examined how individual pyramidal cells (recruited in ensembles) behave upon mild metabolic stress compared to their activity during baseline gamma oscillations. In the example shown in Figure 13, we observed an increase in the activity of pyramidal cells (Figure 13I). We next normalized the activity of individual cells (during baseline or metabolic stress) to the average activity of their corresponding ensemble during baseline. This was performed for all cells from all slices. For better visualization, the normalized activity of cells was sorted for both conditions (Figure 3J). The corresponding distributions are shown in Figure 13K. During metabolic stress, a shift towards increased activity is observed (Figure 13K, right).

Although the overall activity of all cells showed no significant difference (Figure 12I), we observed an increase of pyramidal cell activity on the ensemble level during mild metabolic stress. Our findings show that the formation of ensembles is disturbed probably by partial disinhibition of pyramidal cells. To further elucidate the underlying mechanism, we studied the changes in the firing patterns of slow- and fast-spiking units (SSUs, FSUs) in response to metabolic stress.
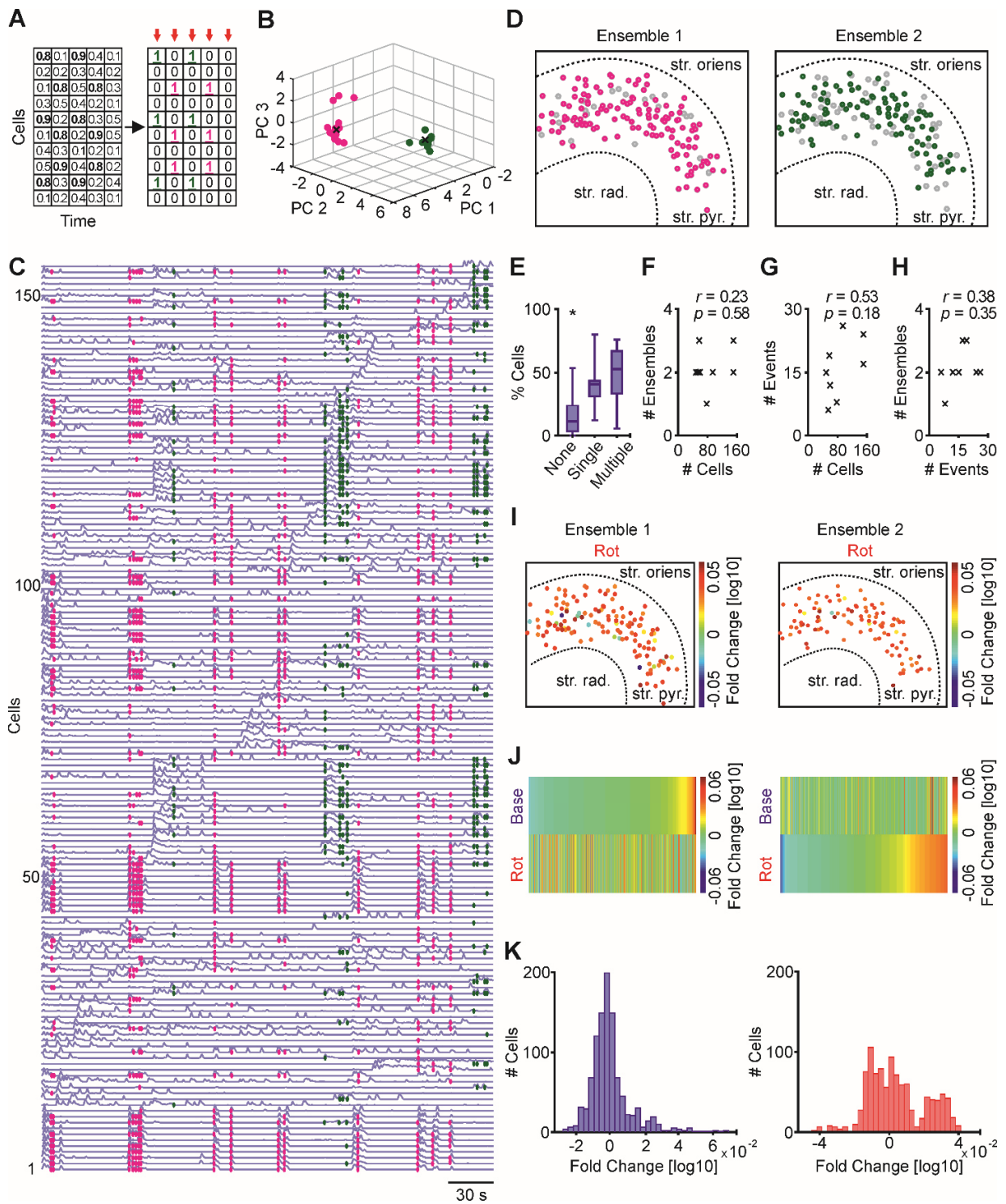
Figure 13. Clustering events of synchronized activity to identify neuronal ensembles. A, Transferring calcium fluorescence transients into binary population vectors (red arrows). **B,** Principal component

analysis applied to categorize vectors in the first three principal components, followed by Fuzzy C-means clustering with the aid of Dunn index (black crosses; the center of clusters). **C,** Traces of calcium fluorescence for all detected cells in one slice with color-coded events according to the ensembles clustered in **B. D,** Spatial map of cells belonging to the two identified ensembles corresponding to the shown example. Data were analyzed for different parameters. n/N slices/preparations: 8/3. Gray circles represent cells not recruited into the presented ensemble. str. oriens, Stratum oriens; str. pyr., Stratum pyramidale; str. rad., Stratum radiatum. **E,** Difference between cells recruited in only one ensemble or multiple ensembles or none. One-way ANOVA with Holm-Sidak's multiple comparisons test, * $p < 0.05$. **F-H,** Correlations between numbers of identified cells, events and ensembles. No significant correlation is observed. **I,** Spatial map (similar to **D**) showing fold change in AuC of cells' activity during mild metabolic stress in relation to their individual activity during baseline gamma oscillations. **J,** Activity of each cell is normalized to the average activity of their corresponding ensemble, followed by sorting according to baseline gamma oscillation (top left) or mild metabolic stress (bottom right). **K,** Histogram of cells' sorted activity (analogous to top left and bottom right in **J**). Note the multimodal distribution (right), and the shift of pyramidal cells to be more active upon mild stress, two-sample Kolmogorov-Smirnov test (D = 0.226, $p < 0.05$). Data are summarized by their median ± the interquartile range (IQR = 75% percentile - 25% percentile), error bars indicate minimal and maximal values.

3.4 Mild metabolic stress disinhibits slow-spiking units

In order to uncover the underlying mechanisms for the observed loss of synchrony, we performed spike sorting with extracellular recordings. The high temporal resolution allows for detecting fast-spiking units (FSU) in addition to slow spiking units (SSU, putative pyramidal cells), thus enabling us to distinguish between their responses to mild metabolic stress.

To achieve similar metabolic stress as in the submerged chamber (Figure 9), rotenone concentration was raised to 0.5 µM. Indeed, gamma oscillations were maintained while power was significantly attenuated (Figure 14). Additionally, none of the slices showed pathological activity (e.g. spreading depolarization or epileptiform discharges), which allowed us to use these conditions to further study the spiking behavior of individual cells.

To extract multi-units activity, we first band-pass (300-3000 Hz) filtered the recorded signals (Figure 15A). Afterward, the identified spikes were sorted based on their wavelet transformations (Quiroga et al., 2004). We were able to distinguish between different units and determined their firing rates (Figure 15B-C). Based on their firing rates, we categorized the units into FSUs (>10 Hz) and SSUs (<5 Hz). While FSUs maintained their firing rate (Figure 15D), SSUs increased their firing rate during mild metabolic stress (Figure 15E). These findings further support our previous observation that pyramidal cells are slightly disinhibited upon mild metabolic stress.
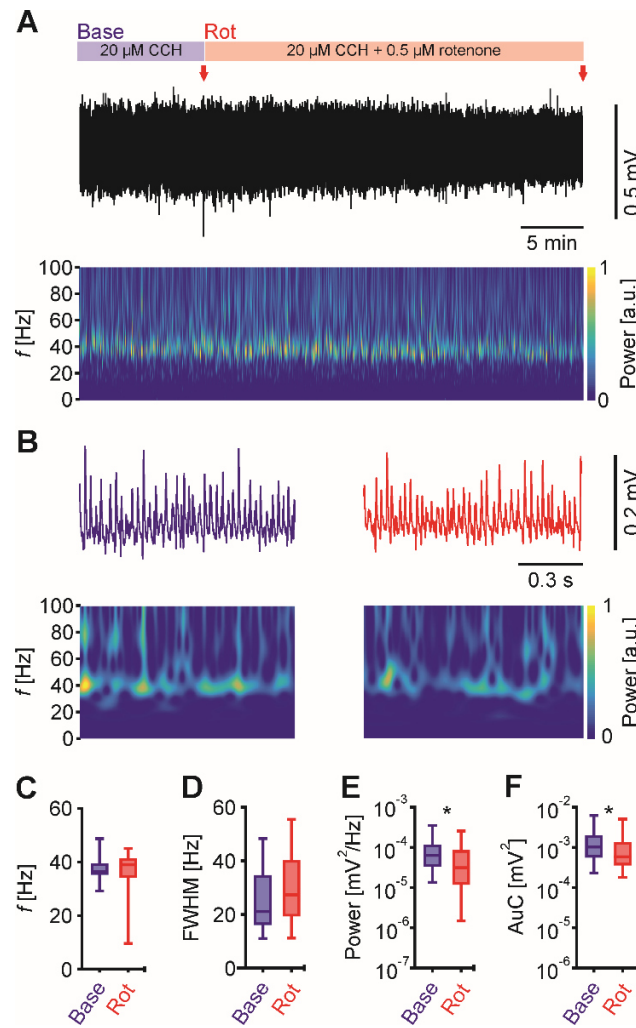
Figure 14. Mild metabolic stress of gamma oscillations in interface condition. A, Sample trace of LFP recording in interface chamber during baseline gamma oscillations (first 10 minutes) and additional application of 0.5 µM rotenone. Red arrows indicate time points in **B** at higher temporal resolution. Corresponding wavelet transformation (bottom) showing the power of frequency domains over time. Heat-scale colors encode for power in arbitrary units (a.u.). Note that wavelet transformations during rotenone application are normalized to transformations during baseline. Gamma oscillations were analyzed for different parameters for the last 5 minutes in each phase (baseline and rotenone application), n/N slices/preparations: 34/6. **C,** Peak frequency (*f*). **D,** Full width at half-maximum (FWHM). **E,** Peak of power spectral density (Power). **F,** Area under the curve (AuC). **C-F**, Wilcoxon matched-pairs signed-rank test. * *p* < 0.05. Data are summarized by their median ± the interquartile range (IQR = 75% percentile - 25% percentile), error bars indicate minimal and maximal values.
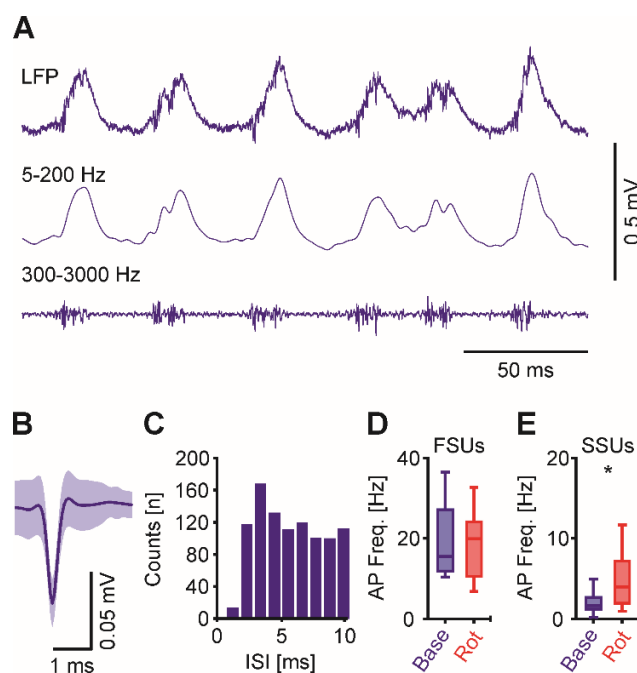
Figure 15. Fast-spiking units are highly vulnerable to mild metabolic stress A, Sample trace of original LFP recording (top), band-pass filtered at 5-200 Hz and 300-3000 Hz (middle and bottom, respectively), highlighting gamma oscillations and units firing. **B**, Sample of a fast-spiking unit, mean ± SD. **C**, Inter-spike interval, ISI for the unit in **B** during baseline gamma oscillations**. D-E,** units/slices/preparations: 18/18 /6. **D,** Action potential (AP) frequency for units with > 10 AP/s during baseline, Wilcoxon matched-pairs signed-rank test. **E,** AP frequency for units with < 5 AP/s during baseline, paired *t*-test. FSUs and SSUs; fast- and slow- spiking units, respectively. * *p* < 0.05. Data are summarized by their median ± the interquartile range (IQR = 75% percentile - 25% percentile), error bars indicate minimal and maximal values.

3.5 CMRO$_2$ in different gamma models and laminae of the hippocampus

In acute hippocampal slices of the mouse, we induced different models of gamma oscillations and performed oxygen depth profiles. We adopted glutamatergic and cholinergic models, using kainic acid (100 nM) and acetylcholine (8 µM) with physostigmine (2 µM), respectively. Persistent oscillations were maintained by constant bath application of the relevant drug in the interface chamber.

In the first set of experiments, we compared the cerebral metabolic rate of oxygen in *stratum pyramidale* of the hippocampus between the two models (Figure 16). Following the oxygen depth profile, a mixture of blockers (0.5 µM TTX, 10 µM DNQX, 50 µM DL-AP5 and 1 µM atropine) was applied to silence neuronal activity. Consequent oxygen depth profiles were performed to serve as a reference for individual slices.

Analysis of the gamma oscillations showed higher power in case of induction using kainic acid. This is reflected in the AuC as well. Frequencies appeared not to be different in both models. However, FWHM was significantly higher in kainic acid-induced gamma oscillations. This implies higher synchrony in the network.

Oxygen consumption is reported after normalizing cerebral metabolic rates during gamma oscillations to rates measured during silenced activity. No difference was detected between the two models.

The second set of experiments involved simultaneous oxygen depth profiles in *stratum pyramidale* and *stratum radiatum*. Only the glutamatergic model was employed; gamma oscillations were induced using kainic acid (Figure 17).

Gamma oscillations in *stratum pyramidale* showed higher amplitudes, reflected in power and AuC. Frequencies showed faster signal in *stratum pyramidale*, additionally, FWHM reflected higher synchrony in the pyramidal layer. Oxygen consumption was significantly higher in the pyramidal layer. This may infer higher energy consumption in *stratum pyramidale* compared to *stratum radiatum*. However, the significant difference can result simply from the significantly more powerful signal in *stratum pyramidale* rather than the nature of the underlying processes (inhibition or excitation).
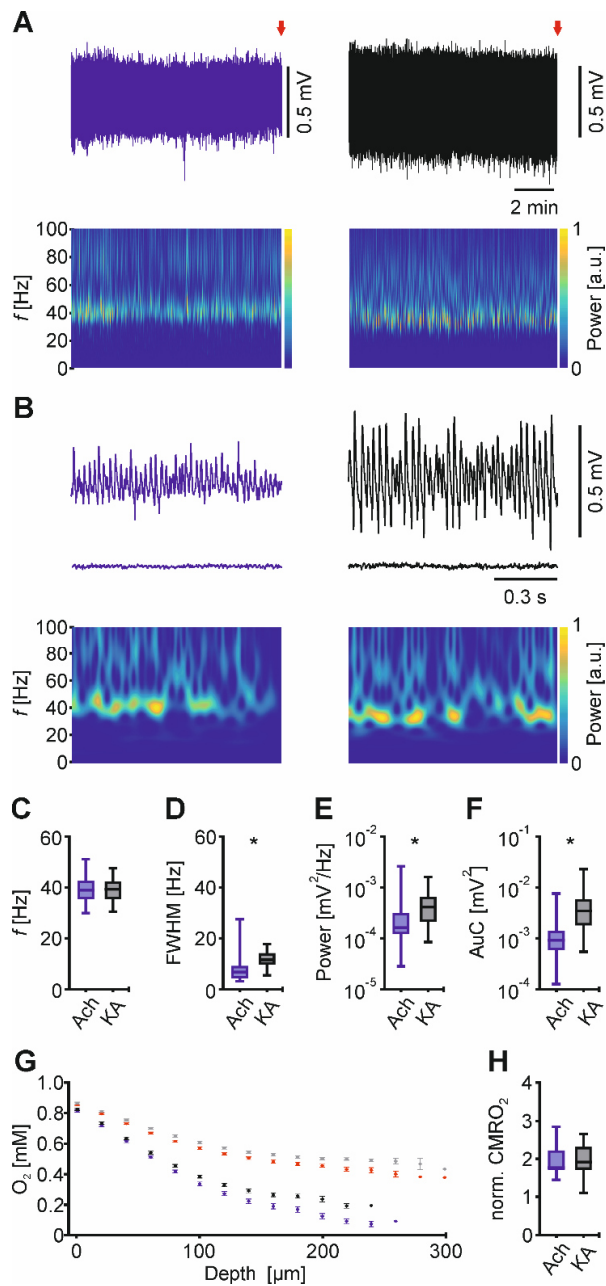
Figure 16. The cerebral metabolic rate of oxygen (CMRO$_2$) in CA3 *stratum pyramidale* of hippocampus. A-B, Sample traces of gamma oscillations induced by acetyl choline and physostigmine (cholinergic model, left), and kainic acid (glutamatergic model, right). Corresponding wavelet transformations (bottom) showing the power of frequency domains over time. Heat-scale colors encode for power in arbitrary units (a.u). Red arrows indicate time points in **B** (top) at higher temporal resolution. **B**, LFP traces (middle) during blocked neuronal activity (TTX + Atropine + DNQX +DL-APV). Bottom, corresponding wavelet transformation for LFPs on top. Gamma oscillations were analyzed for different parameters. For n/N slices/animals: ACh 25/11; KA 27/10. **C**, Peak frequency (*f*), unpaired t-test. **D**, Full width at half-maximum (FWHM). **E**, Peak of power spectral density (Power). **F**, Area under the curve (AuC). **D-F**, Mann-Whitney test. **G**, Oxygen depth profile. Red and grey time series represent profiles of cholinergic and glutamatergic models, respectively after blocking neuronal activity. **H**, normalized CMRO$_2$, Mann-Whitney test. * $p < 0.05$. Data are summarized by their median ± the interquartile range (IQR = 75% percentile - 25% percentile), error bars indicate minimal and maximal values. Calculations of cerebral metabolic rates were performed by Dr. Nikolaus Berndt.
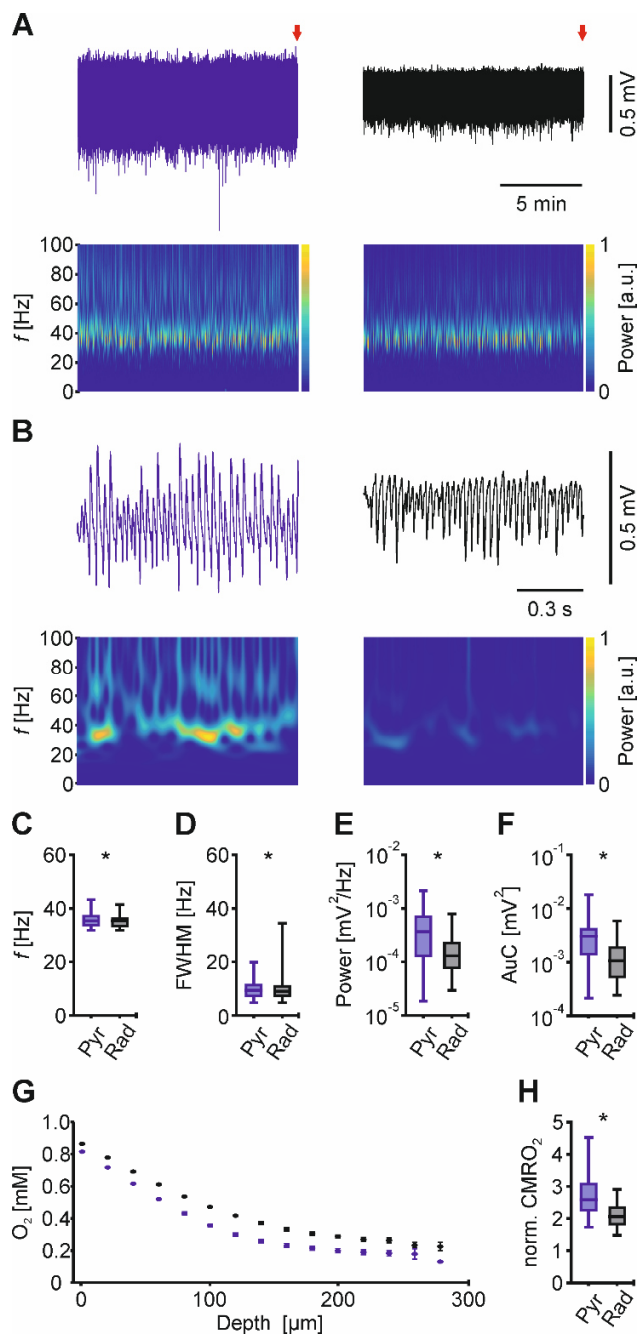
Figure 17. The cerebral metabolic rate of oxygen (CMRO$_2$) in CA3 *stratum pyramidale* (Pyr) and *stratum radiatum* (Rad) of the hippocampus. A-B, Sample traces of gamma oscillations induced by kainic acid in Pyr and Rad, left and right, respectively. Corresponding wavelet transformations (bottom) showing the power of frequency domains over time. Heat-scale colors encode for power in arbitrary units (a.u). Red arrows indicate time points in **B** (top) at higher temporal resolution. **B**, Bottom, corresponding wavelet transformations. Gamma oscillations were analyzed for different parameters. For n/N slices/animals: 33/7. **C**, Peak frequency (*f*), Wilcoxon matched-pairs signed rank test. **D**, Full-width half maximum, Wilcoxon matched-pairs signed rank test. **E**, Peak of power spectral density (Power), Wilcoxon matched-pairs signed rank test. **F**, Area under the curve (AuC), Wilcoxon matched-pairs signed rank test. **G**, Oxygen depth profile. **H**, normalized CMRO$_2$, paired t-test. * p < 0.05. Data are summarized by their median ± the interquartile range (IQR = 75% percentile - 25% percentile), error bars indicate minimal and maximal values. Calculations of cerebral metabolic rates were performed by Dr. Nikolaus Berndt.

48

4 Discussion

4.1 The validity of organotypic hippocampal slice cultures for studying ensembles

Gamma oscillations can be induced *in vitro* by different pharmacological, electrical and optogenetic approaches (Bartos et al., 2007; Kann et al., 2016). In this study, we mainly employed the cholinergic model (carbachol or acetylcholine and physostigmine) of gamma oscillations which mimics cholinergic input from the septum to the hippocampus during exploratory behavior *in vivo* (Fisahn et al., 1998; Hájos and Paulsen, 2009; Marrosu et al., 1995).

Gamma oscillations *in vitro* are known to show comparable properties to the oscillations detected *in vivo*. 1- The phase of gamma oscillations shows a reversal in polarity of LFP between signals recorded from *stratum pyramidale* and *stratum radiatum*. 2- Similar current source density profiles are observed. 3- Low-frequency firing rates of pyramidal cells *in vivo* and *in vitro* during gamma oscillations, ~0.5 - 3 Hz. 4- Similar discharge probabilities of pyramidal cells and inhibitory neurons in correspondence to the phase of the LFP signal (Bartos et al., 2007; Hájos and Paulsen, 2009).

We show in our experiments that gamma oscillations in OHSC have similar properties. This includes the reversal of potential between *stratum pyramidale* and *stratum radiatum* (Figure 3E) and firing rates of pyramidal cells within the range (Figure 12A-B) known from previous studies (Zemankovics et al., 2013). Cross-correlation analysis (Figure 3) revealed that gamma oscillations in the CA3 region precede the signals detected in neighboring regions (dentate gyrus and CA1). Therefore, we conclude that the CA3 in OHSCs is the location where gamma oscillations are generated as known from the literature (Bragin et al., 1995; Csicsvari et al., 2003; Fisahn et al., 1998; Hájos and Paulsen, 2009; Penttonen et al., 1998).

Additionally, former studies presented comparable developmental properties to those observed in the *in-vivo* hippocampus as well as the maturation of interneurons and expression of parvalbumin (Hasam-Henderson et al., 2018; Tsintsadze et al., 2015). Therefore, we conclude that the choice of OHSCs is valid for modeling gamma oscillations *in vitro* and studying underlying network activity.

OHSCs have a residual thickness of ~200 μm (Schneider et al., 2015) offering better diffusion distance for oxygen and metabolites in comparison to acute slices, in addition to the supply of nutrients from beneath the Biopore membrane. For our study, slice cultures are superior to acute slices, since layers of dead cells are removed during the incubation period (Bahr et al., 1995), therefore offering clearer morphology for live imaging. Additionally, the usage OHSCs enabled the application of viral vector carrying a genetically encoded calcium sensor (GECI) under sterile conditions. This provides the additional advantage of transmitting the GECI to all pyramidal cells since the viral vector is applied on top of the slices. The capability of OHSCs to elicit gamma oscillations after more than ~4 weeks (Schneider et al., 2015), provided sufficient incubation period for the expression of the GECI, GCaMP6f, which is known for its fast kinetics (Chen et al., 2013; Podor et al., 2015).

Although gamma oscillations are energetically highly demanding (Huchzermeyer et al., 2013; Kann et al., 2016; Schneider et al., 2017), we were able to induce persistent oscillations in submerged conditions for more than 25 minutes (Figure 8). This duration provided sufficient periods of baseline recordings and induction of metabolic stress that are long enough for robust analysis.

We targeted pyramidal cells by expressing GCaMP6 under the control of CaMKII promoter (Badura et al., 2014; Chen et al., 2013; Podor et al., 2015). Despite the low temporal resolution of calcium imaging, the high spatial resolution enabled identifying and monitoring of large pyramidal cell population simultaneously, permitting detection of neuronal ensembles (Carrillo-Reid et al., 2017; Grienberger and Konnerth, 2012; Hamm et al., 2017; Kwan, 2008).

We developed an algorithm (Figure 11) for reducing cross-talk among different ROIs and combined it with a previously known method for detection of 'above-chance activities' (Hamm et al., 2017; Sasaki et al., 2007). Briefly, the method depends on bootstrapping which is applied to identify above-chance population activity, producing population vectors as an output. Afterward, the vectors are filtered based on their similarity indices to yield only 'repetitive' above-chance activity (Figure 12F). This means that vectors (population activity) consisting of a similar group of

neurons are kept. Thereby fulfilling the definition of ensembles, as a group of repetitively co-active neurons.

Our adopted model of OHSCs and applied algorithms enabled detection of ensembles with simultaneous but not sequential activity (Figure 1). The number of detected active neurons during acquisition time of imaging ranged from 55 up to 155 cells in different slices. A possible explanation could be that intrinsic activity underlying the gamma oscillations show a different number of active neurons at different periods. Another possibility is that the quality of slices is not consistent. Therefore, the reliability of the model was tested to ensure that the quality of slices did not hinder the detection of more active cells or ensembles. We calculated correlations between the number of identified cells, synchronized events, and the number of detected ensembles (Figure 13F-H). We observed that differences in the numbers of detected cells in different slices did not correlate significantly to the number of identified ensembles. In conclusion, we believe that differences in the identified number of cells reflect the underlying intrinsic activity of gamma oscillations rather than unreliable slices quality. Besides, no difference is shown between the numbers of cells recruited in one or multiple ensembles, indicating that a fixed portion of pyramidal cells is active when ensembles are detected (Figure 13E).

The performed characterization of gamma oscillations in OHSCs demonstrates the validity of adopting it as a model for studying neuronal ensembles and their different aspects. We focused in this study on the energetic aspect underlying the formation of pyramidal cell ensembles in the hippocampus.

4.2   Neuroenergetics of gamma oscillations

Research in neuroenergetics has focused mainly on excitatory glutamatergic cells (Attwell and Laughlin, 2001; Hyder et al., 2013; Yu et al., 2017). In the hippocampus, these are the pyramidal cells, which are believed to compute, store and retrieve information during higher brain functions (Hájos and Paulsen, 2009; Lisman and Buzsáki, 2008). Precise temporal windows are necessary for these cells to elicit synchronized activity patterns underlying higher brain functions. However, less focus was given to the inhibitory interneurons which play a key role in providing the temporal windows required for synchronizing pyramidal cells. Main reasons include their low percentage

of neuronal population in the hippocampus (10-15%), and their wide diversity (Gloveli et al., 2005; Somogyi and Klausberger, 2005). Fast-spiking basket cells are of specific interest for synchronizing the activity of pyramidal cells in gamma oscillations (Agetsuma et al., 2018; Gulyás et al., 2010; Hájos and Paulsen, 2009; Penttonen et al., 1998).

Fast-spiking interneurons are able to fire up to 100 Hz. They are endowed with several properties to fulfill this function. This includes: membrane potential with $10 \sim 15$ mV closer to firing threshold compared to pyramidal cells, rapid time course of action potentials, high reliability of action potential propagation along axonal plexus and resonance at frequencies within gamma-frequency band (Hu et al., 2014; Hu and Jonas, 2014; Jonas et al., 2004; Martina et al., 1998; Penttonen et al., 1998; Pike et al., 2000; Sugino et al., 2006). Although interneurons constitute a small percentage of neurons and early estimations suggest their requirement for low energy budget (Attwell and Laughlin, 2001), consideration has to be taken for effects of their massive branching axonal plexus (Caeser and Aertsen, 1991; Freund, 2003; Freund and Buzsáki, 1996). GABAergic interneurons can innervate up to 2000 pyramidal cells, rendering the dissection of neuronal populations of the networks difficult, and consequently determining the most sensitive population to metabolic stress. We approach this issue by challenging pyramidal cell ensembles during gamma oscillations which reflect a highly synchronized activity of neuronal machinery operating at its limit. Inducing mild metabolic stress can, therefore, reveal the most vulnerable population.

4.2.1 Hypoxia as a metabolic stressor

Gamma oscillations and the associated higher cognitive functions are rapidly lost during ischemia due to the required high energy expenditure (Barth and Mody, 2011; Kann, 2012, 2016; Kann et al., 2011; Kann et al., 2014; Schneider et al., 2017). Therefore we simulated the ischemic condition using different combinations of oxygen fractions and glucose concentrations.

Significant changes in the power of gamma oscillations started appearing at 5% oxygen fraction (Figure 5). The changes occurred rapidly and the dynamic phase of metabolic stress lasted for a short period which is insufficient for performing robust analysis. However, interestingly it was noticed that FWHM showed changes when glucose concentration was reduced, and power was

changed only with 5% and 2% oxygen fraction regardless of glucose concentration. FWHM reflects the synchronization of the underlying network activity. Low values indicate a narrow band of frequencies contributing to the detected signal, thereby higher synchrony of neuronal activity and vice versa. Therefore, we further analyzed the isolated effect of glucose concentration and oxygen fractions, to determine if FWHM or power is sensitive more to one of the variables. The analysis of the isolated effect of glucose showed that slice cultures can tolerate reduced concentration and elicit persistent gamma oscillations. Besides, dose-response curves of different oxygen fractions revealed that low fractions showed effect only when combined with low glucose.

We conclude that with the used combinations, we did not detect specific reliance of power or FWHM on oxygen fractions or glucose concentrations, respectively.

4.2.2 Rotenone as a metabolic stressor

We investigated if a pharmacologic stressor would provide a slower dynamic effect, thereby enabling the analysis of longer durations of baseline and stress conditions. We selected rotenone which is a highly selective complex I inhibitor, and its lipophilic nature leads to rapid interference with mitochondrial function and production of ATP (Kann et al., 2003b; Schuchmann et al., 2001; Sherer et al., 2003). We used rotenone in relatively low concentrations, 0.1 μM, and 0.5 μM, in submerged and interface chambers, respectively. At these concentrations, we achieved a mild metabolic stress level, reflected in the reduction of power without loss of gamma-band frequency (Figure 9 and 10). It is essential that stress level is not drastic, otherwise, it will hinder revealing the most vulnerable neuronal population by suppressing the whole network. We note that there was no pathological activity such as spreading depolarization or epileptiform discharges were detected at achieved stress levels.

4.2.3 Synchronized activity exhibits high vulnerability

Changes in synchronized activity were quantified by two parameters. First, the summed durations of synchronized events and second, the number of recruited cells in any synchronized event. These parameters showed significant reduction upon mild metabolic stress as expected (Figure 12). This reflected the disorganized activity of pyramidal cells upon stressing the network.

53

Interestingly, no reduction in the overall activity of pyramidal cells was detected during the stress condition. A possible explanation for this observation is that the stress was mild but sufficient to impair the control of fast-spiking interneurons over pyramidal cells. However, the stress was not sufficient to diminish the activity of pyramidal cells. Another explanation is that the excitatory tone of principle cells upon interneurons is reduced. As a result, the inhibitory control is reduced leading to the observed disorganized activity of pyramidal cells. However, pyramidal cells appeared to have a shift towards higher activity (Figure 13J-K), thus disapproving the second explanation.

These results hence uncover the high energy demands of synchronizing the firing patterns of neurons, which is crucial for information processing. This provides an insight on how the rapid loss of higher cognitive functions upon insults e.g. ischemia occurs.

4.2.4 CMRO$_2$ in different gamma models and laminae of the hippocampus

In this study, we induced gamma oscillations additionally using the glutamatergic model which is based on constant bath application of kainic acid. As known, gamma oscillations involve an interplay between excitatory and inhibitory activity (Hájos and Paulsen, 2009). Previous studies indicated that glutamatergic models of gamma oscillations rely more on inhibition. On the contrary, cholinergic models are dependent more on excitation (Bartos et al., 2007). We exploited this and performed oxygen depth profiles to determine a rough estimate for the energy costs of excitation and inhibition. Oxygen depth profiles provided through a mathematical reaction-diffusion model information about the cerebral metabolic rate of oxygen, CMRO$_2$ (Huchzermeyer et al., 2013; Schneider et al., 2017). Oxygen consumption provides an indirect measure of metabolic rates since it is the final acceptor of electrons in the respiratory chain (Rolfe and Brown, 1997).

The depth profiles were measured in both models of gamma oscillations from the CA3 *stratum pyramidale* where the highest signal power can be detected (Kann et al., 2011).

The observed power and FWHM of gamma oscillations were higher in the glutamatergic model, reflecting a higher level of activity and synchrony underlying the oscillations. Therefore, it was

expected that higher energy consumption is associated with the glutamatergic model and consequently higher $CMRO_2$ levels. However, no significant difference in $CMRO_2$ was detected between the two models. Thereby, it is rendered difficult to confirm that glutamatergic model (which relies mostly on inhibition) is associated with more energy consumption. As a result, we planned thereafter to employ a single model and exploit that different laminae receive different ratios of excitatory and inhibitory inputs.

In the hippocampus, *stratum pyramidale* receive mainly inhibitory inputs and *stratum radiatum* receive excitatory inputs (Megias et al., 2001; Spruston, 2008). Simultaneous recordings of oxygen depth profiles in both layers can provide information on the energy requirement of inhibition and excitation. Comparison of $CMRO_2$ in both layers demonstrated significantly higher values in *stratum pyramidale*, which implies that processes occurring in *stratum pyramidale* are associated with higher energy consumption in comparison to processes in *stratum radiatum*. Consequently, inferring that inhibition costs energetically more than excitation. Taking into consideration the significant difference in gamma oscillations power between *stratum pyramidale* and *stratum radiatum*, the interpretation can be contradicted. Accordingly, the difference in $CMRO_2$ can be attributed to the power of the signal rather than the underlying processes.

Measures of $CMRO_2$ were expected to support our findings from the study of neuronal ensembles which points to high vulnerability of inhibition. Accompanied differences in power and FWHM, which are known to correlate to $CMRO_2$ (Schneider et al., 2017), complicated the interpretation and could contradict any reductionist conclusion.

4.2.5   Interneuron energy hypothesis

It is known that neuronal energy expenditure increases significantly during gamma oscillations (Kann, 2012, 2016; Kann et al., 2014). The strong correlation between gamma oscillations power and oxygen consumption rate (Huchzermeyer et al., 2013; Kann et al., 2011; Schneider et al., 2017), the requirement of high concentration of energy substrates to fuel gamma oscillations (Galow et al., 2014), and the findings of functional imaging in cats, monkeys and humans (Lachaux et al., 2007; Niessing et al., 2005; Schölvinck et al., 2010) support this association.

The remarkable increase in neuronal firings and postsynaptic potentials during gamma oscillations contribute to the high energy budget (Hájos and Paulsen, 2009; Whittington and Traub, 2003; Wong-Riley, 1989). As a consequence of these activities, ion fluxes across neuronal membranes dissipates the gradients of Na^+ K^+ Ca^{2+} and Cl^-. Meanwhile, ion pumps consume energy to restore these gradients by catalyzing ATP (Attwell and Laughlin, 2001; Erecińska and Silver, 2001; Wong-Riley, 1989), which is provided mainly by oxidative phosphorylation in mitochondria (Buzsáki et al., 2007; Kann et al., 2014).

Fast-spiking interneurons also require high energy expenditure. They fire at high rates (> 100 Hz) and are equipped with a large number of mitochondria that are larger in size than pyramidal cells' mitochondria (Gulyás et al., 2006; Gulyas et al., 1999). Additionally, they express supercritical densities of Na^+ channels and fast deactivating Kv3 subtype of K^+ channels, ensuring reliable propagation and fast kinetics of action potentials (Hu et al., 2014; Hu and Jonas, 2014). Furthermore, their mitochondria are enriched with cytochrome C and cytochrome C oxidase, also known as complex IV (Gulyás et al., 2006; Kageyama and Wong-Riley, 1982).

Taking into consideration the findings of previous studies, our results appear to meet expectations. It was anticipated that fast-spiking interneurons will set a low threshold for disturbances of gamma oscillations and inhibition will display high vulnerability.

Fast-spiking interneurons play an important role in feedback and feedforward inhibition rather than just acting as simple breaks for excitatory neurons (Zemankovics et al., 2013). One consequence of feedforward inhibition is the enhancement of the temporal resolution for summation of postsynaptic potentials and initiation of action potentials. As a result, the dynamic range of neuronal ensembles is expanded which is advantageous for information coding (Ferrante et al., 2009; Pouille et al., 2009; Pouille and Scanziani, 2001). Therefore, the observed high vulnerability of fast-spiking interneurons points to one of the functions that will be impaired upon insults to neuronal networks.

4.3   A mechanism for the alteration of gamma oscillations

Fast-spiking interneurons generate action potentials during gamma oscillations, almost phase-locked to each cycle. Therefore, the fast release of GABA leads to rhythmic inhibition in a large population of pyramidal cells. Synchronized inhibitory postsynaptic potentials in *stratum pyramidale* rather than excitatory postsynaptic potentials or action potentials shape the gamma oscillations signal in the LFP (Dugladze et al., 2012; Gloveli et al., 2005; Gulyás et al., 2010; Hájos et al., 2004; Klausberger et al., 2003; Mann et al., 2005; Oren et al., 2010; Penttonen et al., 1998). Consequently, the reduction in gamma oscillations power during mild metabolic stress can result from failures in action potentials generation or propagation along the axons of fast-spiking interneurons. Another possibility is the reduction in GABA released from the presynaptic terminal. It was predicted that energy demand for action potential generation and postsynaptic ion fluxes is higher than the demand of processes occurring at the presynaptic terminal (Attwell and Gibb, 2005; Attwell and Laughlin, 2001; Harris et al., 2012; Howarth et al., 2012). Nevertheless, it was also shown that energy demands for presynaptic processes: Ca^{2+} removal, transmitter release, and uptake and vesicles turnover require more energy than previously expected (Liotta et al., 2012; Rangaraju et al., 2014).

Spike sorting was performed to acquire a deeper insight into the alterations of neuronal firing rates upon metabolic stress. A major issue with spike sorting is clustering. Several algorithms assume a Gaussian shape of clusters. However, there are many causes for non-Gaussian shapes. These include 1- electrode drifting due to slice shrinkage or swelling, 2- correlation between spiking and LFP 3- changes in spike waveform of bursting units 4- the presence of multi-unit activity. Wave_Clus, the algorithm we used, is based on superparamagnetic clustering which is found to overcome the assumption of clusters with Gaussian shape (Blatt et al., 1996; Quiroga et al., 2004; Wild et al., 2012).

Spike sorting showed that slow-spiking units are surprisingly more active during mild metabolic stress. This runs in parallel with the tendency of pyramidal cells to be more active in comparison to the average activity of their corresponding ensemble (Figure 13 J-K). This implies that SSUs are disinhibited and indicates that inhibitory cells are highly vulnerable to mild metabolic stress.

Interestingly, firing rates of fast-spiking units were not affected although gamma oscillations power was significantly reduced. This indicates that the loss of gamma oscillations begins with failures occurring in the presynaptic terminal before changes in firing rates start to appear.

In summary, our findings suggest a high vulnerability of inhibitory cells in gamma oscillations which is a model for neuronal machinery functioning at its limits. This explains the tendency observed in a portion of pyramidal cells being more active (Figure 13 J-K) due to disinhibition when only mild stress is induced.

Furthermore, the presynaptic terminal appears to be the weakest link in a chain of processes involved in synchronizing neuronal population activity. This provides a basic understanding of alterations in gamma oscillations. Additionally, it exposes a plausible mechanism for the pathophysiology of losing higher brain functions in conditions of acute insult such as ischemia or chronic conditions such as aging or Alzheimer's disease (AD).

4.4   Gamma oscillations and brain disorders

Since gamma oscillations are known to be associated with selective attention, memory formation, and sensory perception (Buzsáki and Draguhn, 2004; Colgin, 2016; Colgin and Moser, 2010; Paulsen and Moser, 1998; Uhlhaas and Singer, 2010), it is not surprising that disturbances in gamma oscillations are observed in many brain disorders. This includes AD (Hidisoglu et al., 2018; Hollnagel et al., 2019), schizophrenia (Hamm et al., 2017), ischemia (Barth and Mody, 2011), psychosis (Ahnaou et al., 2017), and depression (Fitzgerald and Watson, 2018). The question remains in these diseases, whether alterations of gamma oscillations are a by-product or are contributing to cognitive impairments.

Several studies showed that improving gamma oscillations lead to a rescuing effect of the pathology of AD (Adaikkan et al., 2019; Iaccarino et al., 2016; Mably and Colgin, 2018). Following optogenetic stimulation of fast-spiking PV+ interneurons, gamma oscillations were enhanced and Aβ plaques were reduced most likely via increased microglial uptake (Iaccarino et al., 2016). Entrainment of gamma oscillations in the visual cortex and hippocampus by non-invasive light flicker and in the auditory cortex by auditory tone stimulation showed similar effects in different

AD mouse models (Adaikkan et al., 2019; Martorell et al., 2019). The pathology of some AD models is known to have disturbed excitation-inhibition balance resulting from the accumulation of peptides such as apolipoprotein E4 and amyloid β (Kurudenkandy et al., 2014; Tong et al., 2014). Overexpression of voltage-gated sodium channel subunit Nav1.1 in interneurons enhanced gamma oscillations and improved the cognitive function in human amyloid precursor protein transgenic mice (Martinez-Losa et al., 2018).

Inducing mild metabolic stress simulates deficiencies in the hemodynamic response which might be responsible for the decline (rather than loss) in cognitive functions. These disturbances occur in Alzheimer's disease, cardiovascular diseases and aging (Love and Miners, 2016; Riddle et al., 2003). They occur as well in mitochondrial diseases associated with impaired mitochondrial function and oxidative stress (Burté et al., 2014; Morán et al., 2012; Zsurka and Kunz, 2013). Studying the neuroenergetic aspect of insults to the brain will help to bridge the gap between cellular damage and cognitive deficits.

4.5   Limitations of the study

Our study provides us with valuable information which helps to understand in depth a rational pathophysiological mechanism for the loss of gamma oscillations which can be related to loss of higher cognitive functions. However, the applied methodology in our study has some limitations.

Although calcium imaging provides an impressive spatial resolution which enables monitoring a large number of neurons, however, the temporal resolution lags behind if compared to other methods such as multi-electrode array recordings of neuronal activity. The algorithms used were designed for calcium imaging data. Nevertheless, the identified ensembles represent co-active neurons with simultaneous activity and lack the full spectrum of ensembles which includes also sequentially active ensembles (Figure 1).

Several factors contribute to the lagging temporal resolution. On the hardware level, this includes the sampling rate which is limited by the specifications of used cameras and exposure time. With new technologies, the limitations are becoming reduced, but this comes with the expense of phototoxicity and photobleaching (Icha et al., 2017; Magidson and Khodjakov, 2013). On the

biological level, the kinetics of the chosen calcium indicator plays an important role. Usually kinetics of sensors are on the scale of hundreds of milliseconds and for some tens of milliseconds, however, neurons fire action potentials on the millisecond scale.

Several algorithms that can identify the broad spectrum of ensembles (sequentially and simultaneously active) are recently published (Russo and Durstewitz, 2017). Nonetheless, to yield the optimal outcome from such modeling algorithms, data with a high temporal and spatial resolution are required.

Spike sorting provides information about firing behavior of detected units, but it has an intrinsic problem which is present in all extracellular recordings intended for spike sorting. The problem is the doubt that comes with the spike sorting process. Major issues include drifting of electrodes, bursting units, overlapping spikes and spiking behavior that is modulated by underlying field potentials (Mokri et al., 2017; Rey et al., 2015). Filtering, spike detection, and clustering are several steps of the process that until now are not standardized to a benchmark (Lewicki, 1998). Several published algorithms tackle these issues, however, no current method can resolve all concerns.

In our study, we suffered an unexpected low yield of sorted units. A possible explanation is the significantly increased activity of neurons during gamma oscillations which renders finding clusters with clear refractory period difficult. Usually, home-built electrodes are of sufficient quality however they lack the standardization of commercial electrodes.

Oxygen sensor recordings offer very fine spatial resolution (8-12 μm). Measures reflect the oxygen utilized by oxidative phosphorylation, the major process in producing ATP. Nevertheless, a reductionist point of view is assumed when interpreting oxygen consumption. The complication arises from the fact that ATP is produced by several other processes (Erecińska and Silver, 2001). Moreover, measured $CMRO_2$ is not necessarily reporting energy consumption of inhibitory or excitatory tone per se, but is also correlated to the power of gamma oscillation as well, which reflects the size of the active neuronal population. Thereby interpretations are made difficult while trying to dissect the processes underlying the reported $CMRO_2$.

4.6 Outlook

Further support for our findings is required. Voltage imaging can provide information about subthreshold activities, excitatory and inhibitory postsynaptic potentials (Bayguinov et al., 2017; Catterall, 2010; Peterka et al., 2011). Such information can provide quantification of the reduction in inhibitory and excitatory tone upon different metabolic stress levels. Furthermore, correlation to LFP can be determined since the gamma oscillation waveform is shaped by subthreshold activities.

ATP imaging combined with optogenetic induction of gamma oscillations will provide information about energetic costs of inhibition and excitation (Lobas et al., 2019; Sohal, 2012; Sohal et al., 2009; Tantama et al., 2013). Channelrhodopsin channels can be targeted to interneurons or pyramidal cells depending on the utilized promoter (Schneider et al., 2015; Sjulson et al., 2016). A necessary requirement is stimulation protocols for the different populations that result in comparable gamma oscillation power. Upon blockage of neuronal transmission (using TTX), ATP can be imaged upon optogenetic stimulation. Thereby we ensure the isolation of excitatory and inhibitory populations while measuring simultaneously ATP changes in the network.

Lastly, to expand the type of ensembles that can be identified and studied (simultaneously and sequentially active), calcium imaging can be combined with high-density multi-electrode arrays (Franke et al., 2012; Ito et al., 2014; Muthmann et al., 2015). Calcium imaging will validate the yield of spike sorting of large neuronal populations, hence acquiring information about spike timings with optimal temporal resolution. Studying the full spectrum of 'ensembles' definition will provide a further understanding of the basic mechanisms of higher cognitive functions from the energetic aspect.

5 Bibliography

Adaikkan, C., Middleton, S. J., Marco, A., Pao, P.-C., Mathys, H., Kim, D. N.-W., Gao, F., Young, J. Z., Suk, H.-J., Boyden, E. S., McHugh, T. J., & Tsai, L.-H. (2019). Gamma entrainment binds higher-order brain regions and offers neuroprotection. *Neuron, 102*(5), 929-943.e928. doi:10.1016/j.neuron.2019.04.011

Adrian, E. D. (1942). Olfactory reactions in the brain of the hedgehog. *The Journal of physiology, 100*(4), 459-473. doi:10.1113/jphysiol.1942.sp003955

Agetsuma, M., Hamm, J. P., Tao, K., Fujisawa, S., & Yuste, R. (2018). Parvalbumin-Positive Interneurons Regulate Neuronal Ensembles in Visual Cortex. *Cerebral Cortex, 28*(5), 1831-1845. doi:10.1093/cercor/bhx169

Ahnaou, A., Huysmans, H., Van de Casteele, T., & Drinkenburg, W. H. I. M. (2017). Cortical high gamma network oscillations and connectivity: a translational index for antipsychotics to normalize aberrant neurophysiological activity. *Translational Psychiatry, 7*(12), 1285. doi:10.1038/s41398-017-0002-9

Aika, Y., Ren, J. Q., Kosaka, K., & Kosaka, T. (1994). Quantitative analysis of GABA-like-immunoreactive and parvalbumin-containing neurons in the CA1 region of the rat hippocampus using a stereological method, the disector. *Experimental brain research, 99*(2), 267-276. doi:10.1007/BF00239593

Ainsworth, M., Lee, S., Cunningham, M. O., Traub, R. D., Kopell, N. J., & Whittington, M. A. (2012). Rates and rhythms: a synergistic view of frequency and temporal coding in neuronal networks. *Neuron, 75*(4), 572-583. doi:10.1016/j.neuron.2012.08.004

Ardiel, E. L., & Rankin, C. H. (2010). An elegant mind: learning and memory in Caenorhabditis elegans. *Learning & Memory, 17*(4), 191-201. doi:10.1101/lm.960510

Attwell, D., & Gibb, A. (2005). Neuroenergetics and the kinetic design of excitatory synapses. *Nature Reviews Neuroscience, 6*(11), 841-849. doi:10.1038/nrn1784

Attwell, D., & Iadecola, C. (2002). The neural basis of functional brain imaging signals. *Trends in Neurosciences, 25*(12), 621-625. doi:10.1016/S0166-2236(02)02264-6

Attwell, D., & Laughlin, S. B. (2001). An energy budget for signaling in the grey matter of the brain. *Journal of cerebral blood flow and metabolism, 21*(10), 1133-1145. doi:10.1097/00004647-200110000-00001

Backus, A. R., Schoffelen, J. M., Szebenyi, S., Hanslmayr, S., & Doeller, C. F. (2016). Hippocampal-Prefrontal Theta Oscillations Support Memory Integration. *Current biology, 26*(4), 450-457. doi:10.1016/j.cub.2015.12.048

Badura, A., Sun, X. R., Giovannucci, A., Lynch, L. A., & Wang, S. S. H. (2014). *Fast calcium sensor proteins for monitoring neural activity* (Vol. 1): SPIE.

Bahr, B. A., Kessler, M., Rivera, S., Vanderklish, P. W., Hall, R. A., Mutneja, M. S., Gall, C., & Hoffman, K. B. (1995). Stable maintenance of glutamate receptors and other synaptic components in long-term hippocampal slices. *Hippocampus, 5*(5), 425-439. doi:10.1002/hipo.450050505

Bak, L. K., Schousboe, A., & Waagepetersen, H. S. (2006). The glutamate/GABA-glutamine cycle: aspects of transport, neurotransmitter homeostasis and ammonia transfer. *Journal of neurochemistry, 98*(3), 641-653. doi:10.1111/j.1471-4159.2006.03913.x

Barth, A. M., & Mody, I. (2011). Changes in hippocampal neuronal activity during and after unilateral selective hippocampal ischemia *in vivo*. *The Journal of Neuroscience, 31*(3), 851-860. doi:10.1523/jneurosci.5080-10.2011

Bartos, M., Vida , I., & Jonas, P. (2007). Synaptic mechanisms of synchronized gamma oscillations in inhibitory interneuron networks. *Nature Reviews Neuroscience, 8*(1), 45-56. doi:10.1038/nrn2044

Bayguinov, P. O., Ma, Y., Gao, Y., Zhao, X., & Jackson, M. B. (2017). Imaging Voltage in Genetically Defined Neuronal Subpopulations with a Cre Recombinase-Targeted Hybrid Voltage Sensor. *The Journal of Neuroscience, 37*(38), 9305-9319. doi:10.1523/jneurosci.1363-17.2017

Berke, J. D., Okatan, M., Skurski, J., & Eichenbaum, H. B. (2004). Oscillatory entrainment of striatal neurons in freely moving rats. *Neuron, 43*(6), 883-896. doi:10.1016/j.neuron.2004.08.035

Berron, D., Schutze, H., Maass, A., Cardenas-Blanco, A., Kuijf, H. J., Kumaran, D., & Duzel, E. (2016). Strong Evidence for Pattern Separation in Human Dentate Gyrus. *The Journal of Neuroscience, 36*(29), 7569-7579. doi:10.1523/jneurosci.0518-16.2016

Blatt, M., Wiseman, S., & Domany, E. (1996). Superparamagnetic clustering of data. *Physical review letters, 76*(18), 3251-3254. doi:10.1103/PhysRevLett.76.3251

Borgers, C., & Kopell, N. (2003). Synchronization in networks of excitatory and inhibitory neurons with sparse, random connectivity. *Neural computation, 15*(3), 509-538. doi:10.1162/089976603321192059

Bragin, A., Jando, G., Nadasdy, Z., Hetke, J., Wise, K., & Buzsaki, G. (1995). Gamma (40-100 Hz) oscillation in the hippocampus of the behaving rat. *The Journal of Neuroscience, 15*(1 Pt 1), 47-60. doi:10.1523/JNEUROSCI.15-01-00047.1995

Brunel, N., & Wang, X. J. (2003). What determines the frequency of fast network oscillations with irregular neural discharges? I. Synaptic dynamics and excitation-inhibition balance. *Journal of neurophysiology, 90*(1), 415-430. doi:10.1152/jn.01095.2002

Bucurenciu, I., Bischofberger, J., & Jonas, P. (2010). A small number of open Ca2+ channels trigger transmitter release at a central GABAergic synapse. *Nature Neuroscience, 13*(1), 19-21. doi:10.1038/nn.2461

Bucurenciu, I., Kulik, A., Schwaller, B., Frotscher, M., & Jonas, P. (2008). Nanodomain coupling between Ca2+ channels and Ca2+ sensors promotes fast and efficient transmitter release at a cortical GABAergic synapse. *Neuron, 57*(4), 536-545. doi:10.1016/j.neuron.2007.12.026

Burté, F., Carelli, V., Chinnery, P. F., & Yu-Wai-Man, P. (2014). Disturbed mitochondrial dynamics and neurodegenerative disorders. *Nature Reviews Neurology, 11*, 11. doi:10.1038/nrneurol.2014.228

Buzsáki, G. (2010). Neural syntax: cell assemblies, synapsembles, and readers. *Neuron, 68*(3), 362-385. doi:10.1016/j.neuron.2010.09.023

Buzsáki, G., & Draguhn, A. (2004). Neuronal oscillations in cortical networks. *Science, 304*(5679), 1926-1929. doi:10.1126/science.1099745

Buzsáki, G., Kaila, K., & Raichle, M. (2007). Inhibition and brain work. *Neuron, 56*(5), 771-783. doi:10.1016/j.neuron.2007.11.008

Buzsáki, G., Leung, L. W., & Vanderwolf, C. H. (1983). Cellular bases of hippocampal EEG in the behaving rat. *Brain research, 287*(2), 139-171. doi:10.1016/0165-0173(83)90037-1

Buzsáki, G., & Wang, X.-J. (2012). Mechanisms of gamma oscillations. *Annual Review of Neuroscience, 35*, 203-225. doi:10.1146/annurev-neuro-062111-150444

Caeser, M., & Aertsen, A. (1991). Morphological organization of rat hippocampal slice cultures. *The Journal of comparative neurology, 307*(1), 87-106. doi:10.1002/cne.903070109

Cajal, S. R. Y. (1899). *Histologie Du Système Nerveux de l'Homme Et Des Vertébrés*: Hachette Livre - BNF.

Cardin, J. A., Carlen, M., Meletis, K., Knoblich, U., Zhang, F., Deisseroth, K., Tsai, L. H., & Moore, C. I. (2009). Driving fast-spiking cells induces gamma rhythm and controls sensory responses. *Nature, 459*(7247), 663-667. doi:10.1038/nature08002

Carrillo-Reid, L., Yang, W., Kang Miller, J. E., Peterka, D. S., & Yuste, R. (2017). Imaging and Optically Manipulating Neuronal Ensembles. *Annual Review of Biophysics, 46*, 271-293. doi:10.1146/annurev-biophys-070816-033647

Catterall, W. A. (2010). Ion channel voltage sensors: structure, function, and pathophysiology. *Neuron, 67*(6), 915-928. doi:10.1016/j.neuron.2010.08.021

Chamma, I., Chevy, Q., Poncer, J. C., & Levi, S. (2012). Role of the neuronal K-Cl co-transporter KCC2 in inhibitory and excitatory neurotransmission. *Frontiers in Cellular Neuroscience, 6*, 5. doi:10.3389/fncel.2012.00005

Chen, T. W., Wardill, T. J., Sun, Y., Pulver, S. R., Renninger, S. L., Baohan, A., Schreiter, E. R., Kerr, R. A., Orger, M. B., Jayaraman, V., Looger, L. L., Svoboda, K., & Kim, D. S. (2013). Ultrasensitive fluorescent proteins for imaging neuronal activity. *Nature, 499*(7458), 295-300. doi:10.1038/nature12354

Chih, C.-P., Lipton, P., & Roberts, E. L., Jr. (2001). Do active cerebral neurons really use lactate rather than glucose? *Trends in Neurosciences, 24*(10), 573-578. doi:10.1016/S0166-2236(00)01920-2

Chrobak, J. J., & Buzsáki, G. (1998). Gamma oscillations in the entorhinal cortex of the freely behaving rat. *The Journal of Neuroscience, 18*(1), 388-398. doi:10.1523/JNEUROSCI.18-01-00388.1998

Colgin, L. L. (2016). Rhythms of the hippocampal network. *Nature Reviews Neuroscience, 17*(4), 239-249. doi:10.1038/nrn.2016.21

Colgin, L. L., & Moser, E. I. (2010). Gamma oscillations in the hippocampus. *Physiology (Bethesda), 25*(5), 319-329. doi:10.1152/physiol.00021.2010

Csicsvari, J., Jamieson , B., Wise, K. D., & Buzsáki, G. (2003). Mechanisms of gamma oscillations in the hippocampus of the behaving rat. *Neuron, 37*(2), 311-322. doi:10.1016/S0896-6273(02)01169-8

DeFelipe, J., López-Cruz, P. L., Benavides-Piccione, R., Bielza, C., Larrañaga, P., Anderson, S., Burkhalter, A., Cauli, B., Fairén, A., Feldmeyer, D., Fishell, G., Fitzpatrick, D., Freund, T. F., González-Burgos, G., Hestrin, S., Hill, S., Hof, P. R., Huang, J., Jones, E. G., Kawaguchi, Y., Kisvárday, Z., Kubota, Y., Lewis, D. A., Marín, O., Markram, H., McBain, C. J., Meyer, H. S., Monyer, H., Nelson, S. B., Rockland, K., Rossier, J., Rubenstein, J. L. R., Rudy, B., Scanziani, M., Shepherd, G. M., Sherwood, C. C., Staiger, J. F., Tamás, G., Thomson, A., Wang, Y., Yuste, R., & Ascoli, G. A. (2013). New insights into the classification and nomenclature of cortical GABAergic interneurons. *Nature Reviews Neuroscience, 14*, 202. doi:10.1038/nrn3444

Díaz-García, C. M., Mongeon, R., Lahmann, C., Koveal, D., Zucker, H., & Yellen, G. (2017). Neuronal Stimulation Triggers Neuronal Glycolysis and Not Lactate Uptake. *Cell Metabolism, 26*(2), 361-374.e364. doi:10.1016/j.cmet.2017.06.021

Diaz-Garcia, C. M., & Yellen, G. (2019). Neurons rely on glucose rather than astrocytic lactate during stimulation. *Journal of neuroscience research, 97*(8), 883-889. doi:10.1002/jnr.24374

Dugladze, T., Schmitz, D., Whittington, M. A., Vida, I., & Gloveli, T. (2012). Segregation of axonal and somatic activity during fast network oscillations. *Science, 336*(6087), 1458-1461. doi:10.1126/science.1222017

Durstewitz, D., Vittoz, N. M., Floresco, S. B., & Seamans, J. K. (2010). Abrupt transitions between prefrontal neural ensemble states accompany behavioral transitions during rule learning. *Neuron, 66*(3), 438-448. doi:10.1016/j.neuron.2010.03.029

Eggermann, E., Bucurenciu, I., Goswami, S. P., & Jonas, P. (2011). Nanodomain coupling between Ca(2)(+) channels and sensors of exocytosis at fast mammalian synapses. *Nature Reviews Neuroscience, 13*(1), 7-21. doi:10.1038/nrn3125

Einevoll, G. T., Kayser, C., Logothetis, N. K., & Panzeri, S. (2013). Modelling and analysis of local field potentials for studying the function of cortical circuits. *Nature Reviews Neuroscience, 14*(11), 770-785. doi:10.1038/nrn3599

Engel, A. K., Fries, P., & Singer, W. (2001). Dynamic predictions: oscillations and synchrony in top-down processing. *Nature Reviews Neuroscience, 2*(10), 704-716. doi:10.1038/35094565

Erecińska, M., & Silver, I. A. (2001). Tissue oxygen tension and brain sensitivity to hypoxia. *Respiration physiology, 128*(3), 263-276. doi:10.1016/S0034-5687(01)00306-1

Ermentrout, G. B., & Kopell, N. (1998). Fine structure of neural spiking and synchronization in the presence of conduction delays. *PNAS, 95*(3), 1259-1264. doi:10.1073/pnas.95.3.1259

Faghihi, F., & Moustafa, A. A. (2017). Combined Computational Systems Biology and Computational Neuroscience Approaches Help Develop of Future "Cognitive Developmental Robotics". *Frontiers in neurorobotics, 11*, 63. doi:10.3389/fnbot.2017.00063

Fellous, J.-M., & Sejnowski, T. J. (2000). Cholinergic induction of oscillations in the hippocampal slice in the slow (0.5-2 Hz), theta (5-12 Hz), and gamma (35-70 Hz) bands. *Hippocampus, 10*(2), 187-197. doi:10.1002/(SICI)1098-1063(2000)10:2<187::AID-HIPO8>3.0.CO;2-M

Ferrante, M., Migliore, M., & Ascoli, G. A. (2009). Feed-forward inhibition as a buffer of the neuronal input-output relation. *PNAS, 106*(42), 18004-18009. doi:10.1073/pnas.0904784106

Fisahn, A., Contractor, A., Traub, R. D., Buhl, E. H., Heinemann, S. F., & McBain, C. J. (2004). Distinct roles for the kainate receptor subunits GluR5 and GluR6 in kainate-induced

hippocampal gamma oscillations The Journal of Neuroscience, *24*(43), 9658-9668. doi:10.1523/JNEUROSCI.2973-04.2004

Fisahn, A., Pike, F. G., Buhl, E. H., & Paulsen, O. (1998). Cholinergic induction of network oscillations at 40 Hz in the hippocampus *in vitro*. *Nature, 394*(6689), 186-189. doi:10.1038/28179

Fisahn, A., Yamada, M., Duttaroy, A., Gan, J.-W., Deng, C.-X., McBain, C. J., & Wess, J. (2002). Muscarinic induction of hippocampal gamma oscillations requires coupling of the M1 receptor to two mixed cation currents. *Neuron, 33*(4), 615-624. doi:10.1016/S0896-6273(02)00587-1

Fitzgerald, P. J., & Watson, B. O. (2018). Gamma oscillations as a biomarker for major depression: an emerging topic. *Translational Psychiatry, 8*(1), 177. doi:10.1038/s41398-018-0239-y

Forster, E., Zhao, S., & Frotscher, M. (2006). Laminating the hippocampus. *Nature Reviews Neuroscience, 7*(4), 259-267. doi:10.1038/nrn1882

Franke, F., Jäckel, D., Dragas, J., Müller, J., Radivojevic, M., Bakkum, D., & Hierlemann, A. (2012). High-density microelectrode array recordings and real-time spike sorting for closed-loop experiments: an emerging technology to study neural plasticity. *Frontiers in Neural Circuits, 6*(105). doi:10.3389/fncir.2012.00105

Freund, T. F. (2003). Interneuron Diversity series: Rhythm and mood in perisomatic inhibition. *Trends in Neurosciences, 26*(9), 489-495. doi:10.1016/s0166-2236(03)00227-3

Freund, T. F., & Buzsáki, G. (1996). Interneurons of the hippocampus. *Hippocampus, 6*(4), 347-470. doi:10.1002/(sici)1098-1063(1996)6:4<347::Aid-hipo1>3.0.Co;2-i

Gähwiler, B. H., Capogna, M., Debanne, D., McKinney, R. A., & Thompson, S. M. (1997). Organotypic slice cultures: a technique has come of age. *Trends in Neurosciences, 20*(10), 471-477. doi:10.1016/S0166-2236(97)01122-3

Galow, L. V., Schneider, J., Lewen, A., Ta, T.-T., Papageorgiou, I. E., & Kann, O. (2014). Energy substrates that fuel fast neuronal network oscillations. *Frontiers in Neuroscience, 8*, 398. doi:10.3389/fnins.2014.00398

Geisler, C., Brunel, N., & Wang, X. J. (2005). Contributions of intrinsic membrane dynamics to fast network oscillations with irregular neuronal discharges. *Journal of neurophysiology, 94*(6), 4344-4361. doi:10.1152/jn.00510.2004

Gloveli, T., Dugladze, T., Saha, S., Monyer, H., Heinemann, U., Traub, R. D., Whittington, M. A., & Buhl, E. H. (2005). Differential involvement of oriens/pyramidale interneurones in hippocampal network oscillations *in vitro*. *The Journal of physiology, 562*(1), 131-147. doi:10.1113/jphysiol.2004.073007

Goldberg, E. M., Watanabe, S., Chang, S. Y., Joho, R. H., Huang, Z. J., Leonard, C. S., & Rudy, B. (2005). Specific functions of synaptically localized potassium channels in synaptic transmission at the neocortical GABAergic fast-spiking cell synapse. *The Journal of Neuroscience, 25*(21), 5230-5235. doi:10.1523/jneurosci.0722-05.2005

Grienberger, C., & Konnerth, A. (2012). Imaging calcium in neurons. *Neuron, 73*(5), 862-885. doi:10.1016/j.neuron.2012.02.011

Grillner, S., & Wallen, P. (1985). Central pattern generators for locomotion, with special reference to vertebrates. *Annual Review of Neuroscience, 8*, 233-261. doi:10.1146/annurev.ne.08.030185.001313

Gulyás, A. I., Buzsáki, G., Freund, T. F., & Hirase, H. (2006). Populations of hippocampal inhibitory neurons express different levels of cytochrome *c*. *European journal of neuroscience, 23*(10), 2581-2594. doi:10.1111/j.1460-9568.2006.04814.x

Gulyas, A. I., Megias, M., Emri, Z., & Freund, T. F. (1999). Total number and ratio of excitatory and inhibitory synapses converging onto single interneurons of different types in the CA1 area of the rat hippocampus. *The Journal of Neuroscience, 19*(22), 10082-10097. doi:10.1523/JNEUROSCI.19-22-10082.1999

Gulyás, A. I., Szabó, G. G., Ulbert, I., Holderith, N., Monyer, H., Erdélyi, F., Szabó, G., Freund, T. F., & Hájos, N. (2010). Parvalbumin-containing fast-spiking basket cells generate the field potential oscillations induced by cholinergic receptor activation in the hippocampus. *The Journal of Neuroscience, 30*(45), 15134-15145. doi:10.1523/JNEUROSCI.4104-10.2010.

Guzman, S. J., Schlogl, A., Frotscher, M., & Jonas, P. (2016). Synaptic mechanisms of pattern completion in the hippocampal CA3 network. *Science, 353*(6304), 1117-1123. doi:10.1126/science.aaf1836

Haider, B., & McCormick, D. A. (2009). Rapid neocortical dynamics: cellular and network mechanisms. *Neuron, 62*(2), 171-189. doi:10.1016/j.neuron.2009.04.008

Hájos, N., Katona, I., Naiem, S. S., MacKie, K., Ledent, C., Mody, I., & Freund, T. F. (2000). Cannabinoids inhibit hippocampal GABAergic transmission and network oscillations. *European journal of neuroscience, 12*(9), 3239-3249. doi:10.1046/j.1460-9568.2000.00217.x

Hájos, N., Palhalmi, J., Mann, E. O., Nemeth, B., Paulsen, O., & Freund, T. F. (2004). Spike timing of distinct types of GABAergic interneuron during hippocampal gamma oscillations *in vitro*. *Journal of Neuroscience, 24*(41), 9127-9137. doi:10.1523/jneurosci.2113-04.2004

Hájos, N., & Paulsen, O. (2009). Network mechanisms of gamma oscillations in the CA3 region of the hippocampus. *Neural Networks, 22*(8), 1113-1119. doi:10.1016/j.neunet.2009.07.024

Halasy, K., & Somogyi, P. (1993). Distribution of GABAergic synapses and their targets in the dentate gyrus of rat: a quantitative immunoelectron microscopic analysis. *Journal für Hirnforschung, 34*(3), 299-308.

Halgren, E., Babb, T. L., & Crandall, P. H. (1977). Responses of human limbic neurons to induced changes in blood gases. *Brain research, 132*(1), 43-63. doi:10.1016/0006-8993(77)90705-3

Hamm, J. P., Peterka, D. S., Gogos, J. A., & Yuste, R. (2017). Altered Cortical Ensembles in Mouse Models of Schizophrenia. *Neuron, 94*(1), 153-167.e158. doi:10.1016/j.neuron.2017.03.019

Hansen, A. J. (1985). Effect of anoxia on ion distribution in the brain. *Physiological Reviews, 65*(1), 101-148. doi:10.1152/physrev.1985.65.1.101

Harris, J. J., Jolivet, R., & Attwell, D. (2012). Synaptic energy use and supply. *Neuron, 75*(5), 762-777. doi:10.1016/j.neuron.2012.08.019

Hasam-Henderson, L. A., Gotti, G. C., Mishto, M., Klisch, C., Gerevich, Z., Geiger, J. R. P., & Kovács, R. (2018). NMDA-receptor inhibition and oxidative stress during hippocampal maturation differentially alter parvalbumin expression and gamma-band activity. *Scientific Reports, 8*(1), 9545. doi:10.1038/s41598-018-27830-2

Hasenstaub, A., Shu, Y., Haider, B., Kraushaar, U., Duque, A., & McCormick, D. A. (2005). Inhibitory postsynaptic potentials carry synchronized frequency information in active cortical networks. *Neuron, 47*(3), 423-435. doi:10.1016/j.neuron.2005.06.016

Hefft, S., & Jonas, P. (2005). Asynchronous GABA release generates long-lasting inhibition at a hippocampal interneuron-principal neuron synapse. *Nature Neuroscience, 8*(10), 1319-1328. doi:10.1038/nn1542

Herculano-Houzel, S. (2009). The human brain in numbers: a linearly scaled-up primate brain. *Frontiers in Human Neuroscience, 3*, 31. doi:10.3389/neuro.09.031.2009

Hermann, B., & Seidenberg, M. (2007). Epilepsy and cognition. *Epilepsy currents, 7*(1), 1-6. doi:10.1111/j.1535-7511.2007.00151.x

Hidisoglu, E., Kantar-Gok, D., Er, H., Acun, A. D., & Yargicoglu, P. (2018). Alterations in spontaneous delta and gamma activity might provide clues to detect changes induced by amyloid-beta administration. *European Journal of Neuroscience, 47*(8), 1013-1023. doi:10.1111/ejn.13832

Hollnagel, J. O., Elzoheiry, S., Gorgas, K., Kins, S., Beretta, C. A., Kirsch, J., Kuhse, J., Kann, O., & Kiss, E. (2019). Early alterations in hippocampal perisomatic GABAergic synapses and network oscillations in a mouse model of Alzheimer's disease amyloidosis. *PLoS One, 14*(1), e0209228. doi:10.1371/journal.pone.0209228

Hoshiba, Y., Wada, T., & Hayashi-Takagi, A. (2017). Synaptic Ensemble Underlying the Selection and Consolidation of Neuronal Circuits during Learning. *Frontiers in Neural Circuits, 11*, 12. doi:10.3389/fncir.2017.00012

Howarth, C., Gleeson, P., & Attwell, D. (2012). Updated energy budgets for neural computation in the neocortex and cerebellum. *Journal of cerebral blood flow and metabolism, 32*(7), 1222-1232. doi:10.1038/jcbfm.2012.35

Hu, H., Gan, J., & Jonas, P. (2014). Interneurons. Fast-spiking, parvalbumin(+) GABAergic interneurons: from cellular design to microcircuit function. *Science, 345*(6196), 1255263. doi:10.1126/science.1255263

Hu, H., & Jonas, P. (2014). A supercritical density of Na^+ channels ensures fast signaling in GABAergic interneuron axons. *Nature Neuroscience, 17*(5), 686-693. doi:nn.3678 [pii];10.1038/nn.3678

Huchzermeyer, C., Albus, K., Gabriel, H.-J., Otáhal, J., Taubenberger, N., Heinemann, U., Kovács, R., & Kann, O. (2008). Gamma oscillations and spontaneous network activity in the hippocampus are highly sensitive to decreases in pO_2 and concomitant changes in mitochondrial redox state. *The Journal of Neuroscience, 28*(5), 1153-1162. doi:10.1523/JNEUROSCI.4105-07.2008

Huchzermeyer, C., Berndt, N., Holzhütter, H.-G., & Kann, O. (2013). Oxygen consumption rates during three different neuronal activity states in the hippocampal CA3 network. *Journal of cerebral blood flow and metabolism, 33*(2), 263-271. doi: 10.1038/jcbfm.2012.165

Hyder, F., Rothman, D. L., & Bennett, M. R. (2013). Cortical energy demands of signaling and nonsignaling components in brain are conserved across mammalian species and activity levels. *PNAS*, 110(9), 3549-3554. doi:10.1073/pnas.1214912110

Iaccarino, H. F., Singer, A. C., Martorell, A. J., Rudenko, A., Gao, F., Gillingham, T. Z., Mathys, H., Seo, J., Kritskiy, O., Abdurrob, F., Adaikkan, C., Canter, R. G., Rueda, R., Brown, E. N., Boyden, E. S., & Tsai, L.-H. (2016). Gamma frequency entrainment attenuates amyloid load and modifies microglia. *Nature, 540*, 230. doi:10.1038/nature20587

Icha, J., Weber, M., Waters, J. C., & Norden, C. (2017). Phototoxicity in live fluorescence microscopy, and how to avoid it. *Bioessays, 39*(8). doi:10.1002/bies.201700003

Ikegaya, Y., Aaron, G., Cossart, R., Aronov, D., Lampl, I., Ferster, D., & Yuste, R. (2004). Synfire chains and cortical songs: temporal modules of cortical activity. *Science, 304*(5670), 559-564. doi:10.1126/science.1093173

Ingram, J., Zhang, C., Cressman, J. R., Hazra, A., Wei, Y., Koo, Y. E., Ziburkus, J., Kopelman, R., Xu, J., & Schiff, S. J. (2014). Oxygen and seizure dynamics: I. Experiments. *Journal of neurophysiology, 112*(2), 205-212. doi:10.1152/jn.00540.2013

Ito, S., Yeh, F.-C., Hiolski, E., Rydygier, P., Gunning, D. E., Hottowy, P., Timme, N., Litke, A. M., & Beggs, J. M. (2014). Large-Scale, High-Resolution Multielectrode-Array Recording Depicts Functional Network Differences of Cortical and Hippocampal Cultures. *PLoS One, 9*(8), e105324. doi:10.1371/journal.pone.0105324

Jonas, P., Bischofberger, J., Fricker, D., & Miles, R. (2004). *Interneuron Diversity series*: Fast in, fast out - temporal and spatial signal processing in hippocampal interneurons. *Trends in Neurosciences, 27*(1), 30-40. doi:S0166-2236(03)00369-2 [pii];10.1016/j.tins.2003.10.010

Joo, H. R., & Frank, L. M. (2018). The hippocampal sharp wave-ripple in memory retrieval for immediate use and consolidation. *Nature Reviews Neuroscience, 19*(12), 744-757. doi:10.1038/s41583-018-0077-1

Kageyama, G. H., & Wong-Riley, M. T. T. (1982). Histochemical localization of cytochrome oxidase in the hippocampus: correlation with specific neuronal types and afferent pathways. *Neuroscience, 7*(10), 2337-2361. doi:10.1016/0306-4522(82)90199-3

Kandel, E. R., Schwartz, J. H., Jessell, T. M., Siegelbaum, S. A., & Hudspeth, A. J. (2012). *Principles of Neural Science, Fifth Edition*: McGraw-Hill Education.

Kann, O. (2012). The energy demand of fast neuronal network oscillations: insights from brain slice preparations. *Frontiers in Pharmacology, 2*, 90. doi:10.3389/fphar.2011.00090

Kann, O. (2016). The interneuron energy hypothesis: Implications for brain disease. *Neurobiology of Disease, 90*, 75-85. doi:10.1016/j.nbd.2015.08.005

Kann, O., Hollnagel, J. O., Elzoheiry, S., & Schneider, J. (2016). Energy and Potassium Ion Homeostasis during Gamma Oscillations. *Frontiers in Molecular Neuroscience, 9*, 47. doi:10.3389/fnmol.2016.00047

Kann, O., Huchzermeyer, C., Kovács, R., Wirtz, S., & Schuelke, M. (2011). Gamma oscillations in the hippocampus require high complex I gene expression and strong functional performance of mitochondria. *Brain, 134*, 345-358. doi:10.1093/brain/awq333

Kann, O., Kovács, R., & Heinemann, U. (2003a). Metabotropic receptor-mediated Ca^{2+} signaling elevates mitochondrial Ca^{2+} and stimulates oxidative metabolism in hippocampal slice cultures. *Journal of Neurophysiology, 90*(2), 613-621. doi:10.1152/jn.00042.2003

Kann, O., Papageorgiou, I. E., & Draguhn, A. (2014). Highly energized inhibitory interneurons are a central element for information processing in cortical networks. *Journal of cerebral blood flow and metabolism, 34*(8), 1270-1282. doi:jcbfm2014104 [pii];10.1038/jcbfm.2014.104

Kann, O., Schuchmann, S., Buchheim, K., & Heinemann, U. (2003b). Coupling of neuronal activity and mitochondrial metabolism as revealed by NAD(P)H fluorescence signals in

organotypic hippocampal slice cultures of the rat. *Neuroscience, 119*(1), 87-100. doi:10.1016/S0306-4522(03)00026-5

Klausberger, T., Magill, P. J., Marton, L. F., Roberts, J. D., Cobden, P. M., Buzsáki, G., & Somogyi, P. (2003). Brain-state- and cell-type-specific firing of hippocampal interneurons *in vivo*. *Nature, 421*(6925), 844-848. doi:10.1038/nature01374

Kraushaar, U., & Jonas, P. (2000). Efficacy and stability of quantal GABA release at a hippocampal interneuron-principal neuron synapse. *The Journal of Neuroscience, 20*(15), 5594-5607. doi:10.1523/JNEUROSCI.20-15-05594.2000

Kurudenkandy, F. R., Zilberter, M., Biverstål, H., Presto, J., Honcharenko, D., Strömberg, R., Johansson, J., Winblad, B., & Fisahn, A. (2014). Amyloid-β-Induced Action Potential Desynchronization and Degradation of Hippocampal Gamma Oscillations Is Prevented by Interference with Peptide Conformation Change and Aggregation. *The Journal of Neuroscience, 34*(34), 11416-11425. doi:10.1523/jneurosci.1195-14.2014

Kwan, A. C. (2008). What can population calcium imaging tell us about neural circuits? *Journal of neurophysiology, 100*(6), 2977-2980. doi:10.1152/jn.91037.2008

Lachaux, J.-P., Fonlupt, P., Kahane, P., Minotti, L., Hoffmann, D., Bertrand, O., & Baciu, M. (2007). Relationship between task-related gamma oscillations and BOLD signal: new insights from combined fMRI and intracranial EEG. *Human Brain Mapping, 28*(12), 1368-1375. doi:10.1002/hbm.20352

LeBeau, F. E. N., Towers, S. K., Traub, R. D., Whittington, M. A., & Buhl, E. H. (2002). Fast network oscillations induced by potassium transients in the rat hippocampus *in vitro*. *The Journal of Physiology, 542*(1), 167-179. doi:10.1113/jphysiol.2002.015933

Lein, P. J., Barnhart, C. D., & Pessah, I. N. (2011). Acute hippocampal slice preparation and hippocampal slice cultures. *Methods in Molecular Biology, 758*, 115-134. doi:10.1007/978-1-61779-170-3_8

Lenck-Santini, P. P., & Scott, R. C. (2015). Mechanisms Responsible for Cognitive Impairment in Epilepsy. *Cold Spring Harbor Perspectives in Medicine, 5*(10). doi:10.1101/cshperspect.a022772

Leung, L. S. (1982). Nonlinear feedback model of neuronal populations in hippocampal CAl region. *Journal of neurophysiology, 47*(5), 845-868. doi:10.1152/jn.1982.47.5.845

Leutgeb, J. K., Leutgeb, S., Moser, M. B., & Moser, E. I. (2007). Pattern separation in the dentate gyrus and CA3 of the hippocampus. *Science, 315*(5814), 961-966. doi:10.1126/science.1135801

Leutgeb, S., & Leutgeb, J. K. (2007). Pattern separation, pattern completion, and new neuronal codes within a continuous CA3 map. *Learning & Memory, 14*(11), 745-757. doi:10.1101/lm.703907

Leutgeb, S., Leutgeb, J. K., Moser, E. I., & Moser, M. B. (2006). Fast rate coding in hippocampal CA3 cell ensembles. *Hippocampus, 16*(9), 765-774. doi:10.1002/hipo.20201

Lewicki, M. S. (1998). A review of methods for spike sorting: the detection and classification of neural action potentials. *Network, 9*(4), R53-78. doi:10.1088/0954-898X_9_4_001

Li, L., Bischofberger, J., & Jonas, P. (2007). Differential gating and recruitment of P/Q-, N-, and R-type Ca2+ channels in hippocampal mossy fiber boutons. *The Journal of Neuroscience, 27*(49), 13420-13429. doi:10.1523/jneurosci.1709-07.2007

Lin, L., Osan, R., & Tsien, J. Z. (2006). Organizing principles of real-time memory encoding: neural clique assemblies and universal neural codes. *Trends in Neurosciences, 29*(1), 48-57. doi:10.1016/j.tins.2005.11.004

Liotta, A., Rosner, J., Huchzermeyer, C., Wojtowicz, A., Kann, O., Schmitz, D., Heinemann, U., & Kovacs, R. (2012). Energy demand of synaptic transmission at the hippocampal Schaffer-collateral synapse. *Journal of cerebral blood flow and metabolism, 32*(11), 2076-2083. doi:10.1038/jcbfm.2012.116

Lisman, J., & Buzsáki, G. (2008). A neural coding scheme formed by the combined function of gamma and theta oscillations. *Schizophrenia Bulletin, 34*(5), 974-980. doi:10.1093/schbul/sbn060

Lisman, J. E. (1999). Relating hippocampal circuitry to function: recall of memory sequences by reciprocal dentate-CA3 interactions. *Neuron, 22*(2), 233-242. doi:S0896-6273(00)81085-5 [pii]

Lobas, M. A., Tao, R., Nagai, J., Kronschläger, M. T., Borden, P. M., Marvin, J. S., Looger, L. L., & Khakh, B. S. (2019). A genetically encoded single-wavelength sensor for imaging cytosolic and cell surface ATP. *Nature Communications, 10*(1), 711. doi:10.1038/s41467-019-08441-5

Love, S., & Miners, J. S. (2016). Cerebrovascular disease in ageing and Alzheimer's disease. *Acta Neuropathologica, 131*(5), 645-658. doi:10.1007/s00401-015-1522-0

Lutas, A., & Yellen, G. (2013). The ketogenic diet: metabolic influences on brain excitability and epilepsy. *Trends in Neurosciences, 36*(1), 32-40. doi:10.1016/j.tins.2012.11.005

Mably, A. J., & Colgin, L. L. (2018). Gamma oscillations in cognitive disorders. *Current Opinion in Neurobiology, 52*, 182-187. doi:10.1016/j.conb.2018.07.009

Magidson, V., & Khodjakov, A. (2013). Circumventing photodamage in live-cell microscopy. *Methods in Cell Biology, 114*, 545-560. doi:10.1016/B978-0-12-407761-4.00023-3

Mainen, Z. F., & Sejnowski, T. J. (1995). Reliability of spike timing in neocortical neurons. *Science, 268*(5216), 1503-1506. doi:10.1126/science.7770778

Mann, E. O., Suckling, J. M., Hájos, N., Greenfield, S. A., & Paulsen, O. (2005). Perisomatic feedback inhibition underlies cholinergically induced fast network oscillations in the rat hippocampus *in vitro*. *Neuron, 45*(1), 105-117. doi:10.1016/j.neuron.2004.12.016

Marrosu, F., Portas, C., Mascia, M. S., Casu, M. A., Fa, M., Giagheddu, M., Imperato, A., & Gessa, G. L. (1995). Microdialysis measurement of cortical and hippocampal acetylcholine release during sleep-wake cycle in freely moving cats. *Brain Research, 671*(2), 329-332. doi:10.1016/0006-8993(94)01399-3

Martina, M., & Jonas, P. (1997). Functional differences in Na+ channel gating between fast-spiking interneurones and principal neurones of rat hippocampus. *The Journal of Physiology, 505 (Pt 3)*, 593-603. doi:10.1111/j.1469-7793.1997.593ba.x

Martina, M., Schultz, J. H., Ehmke, H., Monyer, H., & Jonas, P. (1998). Functional and molecular differences between voltage-gated K+ channels of fast-spiking interneurons and pyramidal neurons of rat hippocampus. *The Journal of Neuroscience, 18*(20), 8111-8125. doi:10.1523/JNEUROSCI.18-20-08111.1998

Martinez-Francois, J. R., Fernandez-Aguera, M. C., Nathwani, N., Lahmann, C., Burnham, V. L., Danial, N. N., & Yellen, G. (2018). BAD and KATP channels regulate neuron excitability and epileptiform activity. *eLife, 7*. doi:10.7554/eLife.32721

Martinez-Losa, M., Tracy, T. E., Ma, K., Verret, L., Clemente-Perez, A., Khan, A. S., Cobos, I., Ho, K., Gan, L., Mucke, L., Alvarez-Dolado, M., & Palop, J. J. (2018). Nav1.1-Overexpressing Interneuron Transplants Restore Brain Rhythms and Cognition in a Mouse Model of Alzheimer's Disease. *Neuron, 98*(1), 75-89.e75. doi:10.1016/j.neuron.2018.02.029

Martorell, A. J., Paulson, A. L., Suk, H.-J., Abdurrob, F., Drummond, G. T., Guan, W., Young, J. Z., Kim, D. N.-W., Kritskiy, O., Barker, S. J., Mangena, V., Prince, S. M., Brown, E. N., Chung, K., Boyden, E. S., Singer, A. C., & Tsai, L.-H. (2019). Multi-sensory Gamma Stimulation Ameliorates Alzheimer's-Associated Pathology and Improves Cognition. *Cell, 177*(2), 256-271.e222. doi:10.1016/j.cell.2019.02.014

McBain, C. J., DiChiara, T. J., & Kauer, J. A. (1994). Activation of metabotropic glutamate receptors differentially affects two classes of hippocampal interneurons and potentiates excitatory synaptic transmission. *The Journal of Neuroscience, 14*(7), 4433-4445. doi:10.1523/JNEUROSCI.14-07-04433.1994

Megias, M., Emri, Z., Freund, T. F., & Gulyas, A. I. (2001). Total number and distribution of inhibitory and excitatory synapses on hippocampal CA1 pyramidal cells. *Neuroscience, 102*(3), 527-540. doi:10.1016/S0306-4522(00)00496-6

Mokri, Y., Salazar, R. F., Goodell, B., Baker, J., Gray, C. M., & Yen, S.-C. (2017). Sorting Overlapping Spike Waveforms from Electrode and Tetrode Recordings. *Frontiers in neuroinformatics, 11*(53). doi:10.3389/fninf.2017.00053

Morán, M., Moreno-Lastres, D., Marín-Buera, L., Arenas, J., Martín, M. A., & Ugalde, C. (2012). Mitochondrial respiratory chain dysfunction: Implications in neurodegeneration. *Free Radical Biology and Medicine, 53*(3), 595-609. doi:10.1016/j.freeradbiomed.2012.05.009

Muthmann, J.-O., Amin, H., Sernagor, E., Maccione, A., Panas, D., Berdondini, L., Bhalla, U. S., & Hennig, M. H. (2015). Spike Detection for Large Neural Populations Using High Density Multielectrode Arrays. *Frontiers in Neuroinformatics, 9*, 28-28. doi:10.3389/fninf.2015.00028

Nanou, E., Lee, A., & Catterall, W. A. (2018). Control of Excitation/Inhibition Balance in a Hippocampal Circuit by Calcium Sensor Protein Regulation of Presynaptic Calcium Channels. *The Journal of Neuroscience, 38*(18), 4430-4440. doi:10.1523/jneurosci.0022-18.2018

Neves, G., Cooke, S. F., & Bliss, T. V. (2008). Synaptic plasticity, memory and the hippocampus: a neural network approach to causality. *Nature Reviews Neuroscience, 9*(1), 65-75. doi:10.1038/nrn2303

Niessing, J., Ebisch, B., Schmidt, K. E., Niessing, M., Singer, W., & Galuske, R. A. W. (2005). Hemodynamic signals correlate tightly with synchronized gamma oscillations. *Science, 309*(5736), 948-951. doi:10.1126/science.1110948

Noraberg, J., Poulsen, F. R., Blaabjerg, M., Kristensen, B. W., Bonde, C., Montero, M., Meyer, M., Gramsbergen, J. B., & Zimmer, J. (2005). Organotypic hippocampal slice cultures for studies of brain damage, neuroprotection and neurorepair. *Current Drug Targets - CNS & Neurological Disorders, 4*(4), 435-452. doi:10.2174/1568007054546108

Nyhus, E., & Curran, T. (2009). Semantic and perceptual effects on recognition memory: evidence from ERP. *Brain Research, 1283*, 102-114. doi:10.1016/j.brainres.2009.05.091

O'Keefe, J., & Recce, M. L. (1993). Phase relationship between hippocampal place units and the EEG theta rhythm. *Hippocampus, 3*(3), 317-330. doi:10.1002/hipo.450030307

Ohiorhenuan, I. E., Mechler, F., Purpura, K. P., Schmid, A. M., Hu, Q., & Victor, J. D. (2010). Sparse coding and high-order correlations in fine-scale cortical networks. *Nature, 466*(7306), 617-621. doi:10.1038/nature09178

Olafsdottir, H. F., Bush, D., & Barry, C. (2018). The Role of Hippocampal Replay in Memory and Planning. *Current Biology, 28*(1), R37-r50. doi:10.1016/j.cub.2017.10.073

Olshausen, B. A., & Field, D. J. (2004). Sparse coding of sensory inputs. *Current Opinion in Neurobiology, 14*(4), 481-487. doi:10.1016/j.conb.2004.07.007

Oren, I., Hájos, N., & Paulsen, O. (2010). Identification of the current generator underlying cholinergically induced gamma frequency field potential oscillations in the hippocampal CA3 region. *The Journal of Physiology, 588*(Pt 5), 785-797. doi:10.1113/jphysiol.2009.180851

Parnas, I., & Segev, I. (1979). A mathematical model for conduction of action potentials along bifurcating axons. *The Journal of Physiology, 295*, 323-343. doi:10.1113/jphysiol.1979.sp012971

Paulsen, O., & Moser, E. I. (1998). A model of hippocampal memory encoding and retrieval: GABAergic control of synaptic plasticity. *Trends in Neurosciences 21*(7), 273-278. doi:S0166223697012058 [pii], doi: 10.1016/S0166-2236(97)01205-8

Penttonen, M., Kamondi, A., Acsady, L., & Buzsáki, G. (1998). Gamma frequency oscillation in the hippocampus of the rat: intracellular analysis *in vivo*. *European journal of Neuroscience, 10*(2), 718-728. doi:10.1046/j.1460-9568.1998.00096.x

Peterka, D. S., Takahashi, H., & Yuste, R. (2011). Imaging voltage in neurons. *Neuron, 69*(1), 9-21. doi:10.1016/j.neuron.2010.12.010

Pike, F. G., Goddard, R. S., Suckling, J. M., Ganter, P., Kasthuri, N., & Paulsen, O. (2000). Distinct frequency preferences of different types of rat hippocampal neurones in response to oscillatory input currents. *The Journal of Physiology, 529 Pt 1*(Pt 1), 205-213. doi:10.1111/j.1469-7793.2000.00205.x

Pinault, D., & Deschenes, M. (1992). Voltage-dependent 40-Hz oscillations in rat reticular thalamic neurons *in vivo*. *Neuroscience, 51*(2), 245-258. doi:10.1016/0306-4522(92)90312-P

Plenz, D., & Thiagarajan, T. C. (2007). The organizing principles of neuronal avalanches: cell assemblies in the cortex? *Trends in Neurosciences, 30*(3), 101-110. doi:10.1016/j.tins.2007.01.005

Podor, B., Hu, Y. L., Ohkura, M., Nakai, J., Croll, R., & Fine, A. (2015). Comparison of genetically encoded calcium indicators for monitoring action potentials in mammalian brain by two-photon excitation fluorescence microscopy. *Neurophotonics, 2*(2), 021014. doi:10.1117/1.NPh.2.2.021014

Popescu, A. T., Popa, D., & Paré, D. (2009). Coherent gamma oscillations couple the amygdala and striatum during learning. *Nature Neuroscience, 12*, 801. doi:10.1038/nn.2305

Poschel, B., Draguhn, A., & Heinemann, U. (2002). Glutamate-induced gamma oscillations in the dentate gyrus of rat hippocampal slices. *Brain Research, 938*(1-2), 22-28. doi:10.1016/S0006-8993(02)02477-0

Pouille, F., Marin-Burgin, A., Adesnik, H., Atallah, B. V., & Scanziani, M. (2009). Input normalization by global feedforward inhibition expands cortical dynamic range. *Nature Neuroscience, 12*(12), 1577-1585. doi:10.1038/nn.2441

Pouille, F., & Scanziani, M. (2001). Enforcement of temporal fidelity in pyramidal cells by somatic feed-forward inhibition. *Science, 293*(5532), 1159-1163. doi:10.1126/science.1060342

Quilichini, P., Sirota, A., & Buzsáki, G. (2010). Intrinsic circuit organization and theta-gamma oscillation dynamics in the entorhinal cortex of the rat. *The Journal of Neuroscience, 30*(33), 11128-11142. doi:10.1523/jneurosci.1327-10.2010

Quiroga, R. Q., Nadasdy, Z., & Ben-Shaul, Y. (2004). Unsupervised spike detection and sorting with wavelets and superparamagnetic clustering. *Neural Computation, 16*(8), 1661-1687. doi:10.1162/089976604774201631

Rangaraju, V., Calloway, N., & Ryan, T. A. (2014). Activity-driven local ATP synthesis is required for synaptic function. *Cell*, 156(4), 825-835. doi:10.1016/j.cell.2013.12.042

Rey, H. G., Pedreira, C., & Quian Quiroga, R. (2015). Past, present and future of spike sorting techniques. *Brain Research Bulletin, 119*, 106-117. doi:10.1016/j.brainresbull.2015.04.007

Riddle, D. R., Sonntag, W. E., & Lichtenwalner, R. J. (2003). Microvascular plasticity in aging. *Ageing Research Reviews, 2*(2), 149-168. doi:10.1016/S1568-1637(02)00064-8

Rolfe, D. F. S., & Brown, G. C. (1997). Cellular energy utilization and molecular origin of standard metabolic rate in mammals. *Physiological Reviews, 77*(3), 731-758. doi:10.1152/physrev.1997.77.3.731

Rolls, E. T. (2013). The mechanisms for pattern completion and pattern separation in the hippocampus. *Frontiers in Systems Neuroscience, 7*, 74. doi:10.3389/fnsys.2013.00074

Rossignol, E., Kruglikov, I., van den Maagdenberg, A. M., Rudy, B., & Fishell, G. (2013). CaV 2.1 ablation in cortical interneurons selectively impairs fast-spiking basket cells and causes generalized seizures. *Annals of Neurology, 74*(2), 209-222. doi:10.1002/ana.23913

Roth, F. C., & Draguhn, A. (2012). GABA metabolism and transport: effects on synaptic efficacy. *Neural Plasticity, 2012*, Article ID 805830-805812 pages. doi:10.1155/2012/805830

Rubin, R., Abbott, L. F., & Sompolinsky, H. (2017). Balanced excitation and inhibition are required for high-capacity, noise-robust neuronal selectivity. *PNAS, 114*(44), E9366-e9375. doi:10.1073/pnas.1705841114

Rudy, B., & McBain, C. J. (2001). Kv3 channels: voltage-gated K+ channels designed for high-frequency repetitive firing. *Trends in Neurosciences, 24*(9), 517-526. doi:10.1016/S0166-2236(00)01892-0

Russo, E., & Durstewitz, D. (2017). Cell assemblies at multiple time scales with arbitrary lag constellations. *eLife, 6*, e19428. doi:10.7554/eLife.19428

Sasaki, T., Matsuki, N., & Ikegaya, Y. (2007). Metastability of active CA3 networks. *The Journal of Neuroscience, 27*(3), 517-528. doi:10.1523/jneurosci.4514-06.2007

Schindelin, J., Arganda-Carreras, I., Frise, E., Kaynig, V., Longair, M., Pietzsch, T., Preibisch, S., Rueden, C., Saalfeld, S., Schmid, B., Tinevez, J. Y., White, D. J., Hartenstein, V., Eliceiri, K., Tomancak, P., & Cardona, A. (2012). Fiji: an open-source platform for biological-image analysis. *Nature Methods, 9*(7), 676-682. doi:10.1038/nmeth.2019

Schneider, F., Grimm, C., & Hegemann, P. (2015). Biophysics of Channelrhodopsin. *Annual Review of Biophysics, 44*(1), 167-186. doi:10.1146/annurev-biophys-060414-034014

Schneider, J., Berndt, N., Papageorgiou, I. E., Maurer, J., Bulik, S., Both, M., Draguhn, A., Holzhutter, H. G., & Kann, O. (2017). Local oxygen homeostasis during various neuronal network activity states in the mouse hippocampus. *Journal of cerebral blood flow and metabolism*, 39(5), 859–873. doi:10.1177/0271678x17740091

Schneider, J., Lewen, A., Ta, T. T., Galow, L. V., Isola, R., Papageorgiou, I. E., & Kann, O. (2015). A reliable model for gamma oscillations in hippocampal tissue. *Journal of Neuroscience research,* 93: 1067-1078. doi:10.1002/jnr.23590

Schölvinck, M. L., Maier, A., Ye, F. Q., Duyn, J. H., & Leopold, D. A. (2010). Neural basis of global resting-state fMRI activity. *PNAS, 107*(22), 10238-10243. doi:0913110107 [pii];10.1073/pnas.0913110107

Schuchmann, S., Kovacs, R., Kann, O., Heinemann, U., & Buchheim, K. (2001). Monitoring NAD(P)H autofluorescence to assess mitochondrial metabolic functions in rat hippocampal-entorhinal cortex slices. *Brain Research Protocols, 7*(3), 267-276. doi:10.1016/S1385-299X(01)00080-0

Sengupta, B., Stemmler, M. B., & Friston, K. J. (2013). Information and efficiency in the nervous system--a synthesis. *PLoS Computational Biology, 9*(7), e1003157. doi:10.1371/journal.pcbi.1003157

Sherer, T. B., Betarbet, R., Testa, C. M., Seo, B. B., Richardson, J. R., Kim, J. H., Miller, G. W., Yagi, T., Matsuno-Yagi, A., & Greenamyre, J. T. (2003). Mechanism of toxicity in rotenone models of Parkinson's disease. *The Journal of Neuroscience, 23*(34), 10756-10764. doi:10.1523/JNEUROSCI.23-34-10756.2003

Shulman, R. G., Hyder, F., & Rothman, D. L. (2001). Lactate efflux and the neuroenergetic basis of brain function. *NMR Biomedicine, 14*(7-8), 389-396. doi:10.1002/nbm.741

Sjulson, L., Cassataro, D., DasGupta, S., & Miesenbock, G. (2016). Cell-Specific Targeting of Genetically Encoded Tools for Neuroscience. *Annual Review of Genetics, 50*, 571-594. doi:10.1146/annurev-genet-120215-035011

Skaggs, W. E., McNaughton, B. L., Wilson, M. A., & Barnes, C. A. (1996). Theta phase precession in hippocampal neuronal populations and the compression of temporal sequences. *Hippocampus, 6*(2), 149-172. doi:10.1002/(sici)1098-1063(1996)6:2<149::Aid-hipo6>3.0.Co;2-k

Sohal, V. S. (2012). Insights into Cortical Oscillations Arising from Optogenetic Studies. *Biological Psychiatry, 71*(12), 1039-1045. doi:10.1016/j.biopsych.2012.01.024

Sohal, V. S., Zhang, F., Yizhar, O., & Deisseroth, K. (2009). Parvalbumin neurons and gamma rhythms enhance cortical circuit performance. *Nature, 459*, 698. doi:10.1038/nature07991

Soltesz, I., & Deschenes, M. (1993). Low- and high-frequency membrane potential oscillations during theta activity in CA1 and CA3 pyramidal neurons of the rat hippocampus under ketamine-xylazine anesthesia. *Journal of Neurophysiology, 70*(1), 97-116. doi:10.1152/jn.1993.70.1.97

Somogyi, P., & Klausberger, T. (2005). Defined types of cortical interneurone structure space and spike timing in the hippocampus. *The Journal of Physiology, 562*(1), 9-26. doi:10.1113/jphysiol.2004.078915

Spruston, N. (2008). Pyramidal neurons: dendritic structure and synaptic integration. *Nature Reviews Neuroscience, 9*, 206. doi:10.1038/nrn2286

Sugino, K., Hempel, C. M., Miller, M. N., Hattox, A. M., Shapiro, P., Wu, C., Huang, Z. J., & Nelson, S. B. (2006). Molecular taxonomy of major neuronal classes in the adult mouse forebrain. *Nature Neuroscience, 9*(1), 99-107. doi:10.1038/nn1618

Tantama, M., Martínez-François, J. R., Mongeon, R., & Yellen, G. (2013). Imaging energy status in live cells with a fluorescent biosensor of the intracellular ATP-to-ADP ratio. *Nature Communications, 4*, 2550-2550. doi:10.1038/ncomms3550

Tong, L. M., Djukic, B., Arnold, C., Gillespie, A. K., Yoon, S. Y., Wang, M. M., Zhang, O., Knoferle, J., Rubenstein, J. L. R., Alvarez-Buylla, A., & Huang, Y. (2014). Inhibitory Interneuron Progenitor Transplantation Restores Normal Learning and Memory in ApoE4 Knock-In Mice without or with Aβ Accumulation. *The Journal of Neuroscience, 34*(29), 9506-9515. doi:10.1523/jneurosci.0693-14.2014

Tort, A. B., Kramer, M. A., Thorn, C., Gibson, D. J., Kubota, Y., Graybiel, A. M., & Kopell, N. J. (2008). Dynamic cross-frequency couplings of local field potential oscillations in rat striatum and hippocampus during performance of a T-maze task. *PNAS, 105*(51), 20517-20522. doi:10.1073/pnas.0810524105

Tsintsadze, V., Minlebaev, M., Suchkov, D., Cunningham, M. O., & Khazipov, R. (2015). Ontogeny of kainate-induced gamma oscillations in the rat CA3 hippocampus *in vitro*. *Frontiers in Cellular Neuroscience, 9*, 195. doi:10.3389/fncel.2015.00195

Tukker, J. J., Lasztóczi, B., Katona, L., Roberts, J. D., Pissadaki, E. K., Dalezios, Y., Márton, L., Zhang, L., Klausberger, T., & Somogyi, P. (2013). Distinct dendritic arborization and *in vivo* firing patterns of parvalbumin-expressing basket cells in the hippocampal area CA3. *The Journal of Neuroscience, 33*(16), 6809-6825. doi: 10.1523/JNEUROSCI.5052-12.2013

Uhlhaas, P. J., & Singer, W. (2010). Abnormal neural oscillations and synchrony in schizophrenia. *Nature Reviews Neuroscience, 11*(2), 100-113. doi: 10.1038/nrn2774.

van Hooft, J. A., Giuffrida, R., Blatow, M., & Monyer, H. (2000). Differential expression of group I metabotropic glutamate receptors in functionally distinct hippocampal interneurons. *The Journal of Neuroscience, 20*(10), 3544-3551. doi:10.1523/JNEUROSCI.20-10-03544.2000

van Vugt, M. K., Schulze-Bonhage, A., Litt, B., Brandt, A., & Kahana, M. J. (2010). Hippocampal gamma oscillations increase with memory load. *The Journal of Neuroscience, 30*(7), 2694-2699. doi:10.1523/JNEUROSCI.0567-09.2010

Verweij, B. H., Amelink, G. J., & Muizelaar, J. P. (2007). Current concepts of cerebral oxygen transport and energy metabolism after severe traumatic brain injury. *Progress in Brain Research, 161*, 111-124. doi:10.1016/S0079-6123(06)61008-X

Vodovozov, W., Schneider, J., Elzoheiry, S., Hollnagel, J. O., Lewen, A., & Kann, O. (2018). Metabolic modulation of neuronal gamma-band oscillations. *Pflügers Archiv, 470*(9), 1377-1389. doi:10.1007/s00424-018-2156-6

Waagepetersen, H. S., Sonnewald, U., Gegelashvili, G., Larsson, O. M., & Schousboe, A. (2001). Metabolic distinction between vesicular and cytosolic GABA in cultured GABAergic neurons using ^{13}C magnetic resonance spectroscopy. *Journal of Neuroscience Research, 63*(4), 347-355. doi:10.1002/1097-4547(20010215)63:4<347::AID-JNR1029>3.0.CO;2-G

Walls, A. B., Eyjolfsson, E. M., Smeland, O. B., Nilsen, L. H., Schousboe, I., Schousboe, A., Sonnewald, U., & Waagepetersen, H. S. (2011). Knockout of GAD65 has major impact on synaptic GABA synthesized from astrocyte-derived glutamine. *Journal of Cerebral Blood Flow and Metabolism, 31*(2), 494-503. doi: 10.1038/jcbfm.2010.115

Wang, X. J., & Buzsáki, G. (1996). Gamma oscillation by synaptic inhibition in a hippocampal interneuronal network model. *The Journal of Neuroscience, 16*(20), 6402-6413. doi:10.1523/JNEUROSCI.16-20-06402.1996

Weiser, M., Bueno, E., Sekirnjak, C., Martone, M. E., Baker, H., Hillman, D., Chen, S., Thornhill, W., Ellisman, M., & Rudy, B. (1995). The potassium channel subunit KV3.1b is localized to

somatic and axonal membranes of specific populations of CNS neurons. *The Journal of Neuroscience, 15*(6), 4298-4314. doi:10.1523/JNEUROSCI.15-06-04298.1995

Whishaw, I. Q., & Kolb, B. (2004). *The Behavior of the Laboratory Rat: A Handbook with Tests*: Oxford University Press.

Whittington, M. A., & Traub, R. D. (2003). *Interneuron diversity series*: Inhibitory interneurons and network oscillations *in vitro*. *Trends in Neurosciences, 26*(12), 676-682. doi:10.1016/j.tins.2003.09.016

Whittington, M. A., Traub, R. D., & Jefferys, J. G. R. (1995). Synchronized oscillations in interneuron networks driven by metabotropic glutamate receptor activation. *Nature, 373*(6515), 612-615. doi:10.1038/373612a0

Wild, J., Prekopcsak, Z., Sieger, T., Novak, D., & Jech, R. (2012). Performance comparison of extracellular spike sorting algorithms for single-channel recordings. *Journal of Neuroscience Methods, 203*(2), 369-376. doi:10.1016/j.jneumeth.2011.10.013

Williams, R. W., & Herrup, K. (1988). The control of neuron number. *Annual Review of Neuroscience, 11*, 423-453. doi:10.1146/annurev.ne.11.030188.002231

Wilson, H. R., & Cowan, J. D. (1972). Excitatory and inhibitory interactions in localized populations of model neurons. *Biophysical journal, 12*(1), 1-24. doi:10.1016/s0006-3495(72)86068-5

Wong-Riley, M. T. T. (1989). Cytochrome oxidase: an endogenous metabolic marker for neuronal activity. *Trends in Neurosciences, 12*(3), 94-101. doi:10.1016/0166-2236(89)90165-3

Yellen, G. (2018). Fueling thought: Management of glycolysis and oxidative phosphorylation in neuronal metabolism. *The Journal of Cell Biology, 217*(7), 2235-2246. doi:10.1083/jcb.201803152

Yu, Y., Herman, P., Rothman, D. L., Agarwal, D., & Hyder, F. (2017). Evaluating the gray and white matter energy budgets of human brain function. *Journal of Cerebral Blood Flow and Metabolism*, 271678X17708691. doi:10.1177/0271678X17708691

Zaitsev, A. V., Povysheva, N. V., Lewis, D. A., & Krimer, L. S. (2007). P/Q-type, but not N-type, calcium channels mediate GABA release from fast-spiking interneurons to pyramidal cells in rat prefrontal cortex. *Journal of Neurophysiology, 97*(5), 3567-3573. doi:10.1152/jn.01293.2006

Zarnadze, S., Bauerle, P., Santos-Torres, J., Bohm, C., Schmitz, D., Geiger, J. R., Dugladze, T., & Gloveli, T. (2016). Cell-specific synaptic plasticity induced by network oscillations. *eLife, 5*. doi:10.7554/eLife.14912

Zemankovics, R., Veres, J. M., Oren, I., & Hájos, N. (2013). Feedforward Inhibition Underlies the Propagation of Cholinergically Induced Gamma Oscillations from Hippocampal CA3 to CA1. *The Journal of Neuroscience, 33*(30), 12337-12351. doi:10.1523/jneurosci.3680-12.2013

Zenke, F., Hennequin, G., & Gerstner, W. (2013). Synaptic plasticity in neural networks needs homeostasis with a fast rate detector. *PLoS Computational Biology, 9*(11), e1003330. doi:10.1371/journal.pcbi.1003330

Zsurka, G., & Kunz, W. S. (2013). Mitochondrial involvement in neurodegenerative diseases. *IUBMB Life, 65*(3), 263-272. doi:10.1002/iub.1126